LBNL-41558
Preprint

ERNEST ORLANDO LAWRENCE
BERKELEY NATIONAL LABORATORY

The Intensification of Two-Dimensional Swirling Flows by Stochastic Asymmetric Forcing

David S. Nolan

Computing Sciences Directorate

March 1998

Submitted to
Journal of the Atmospheric Sciences

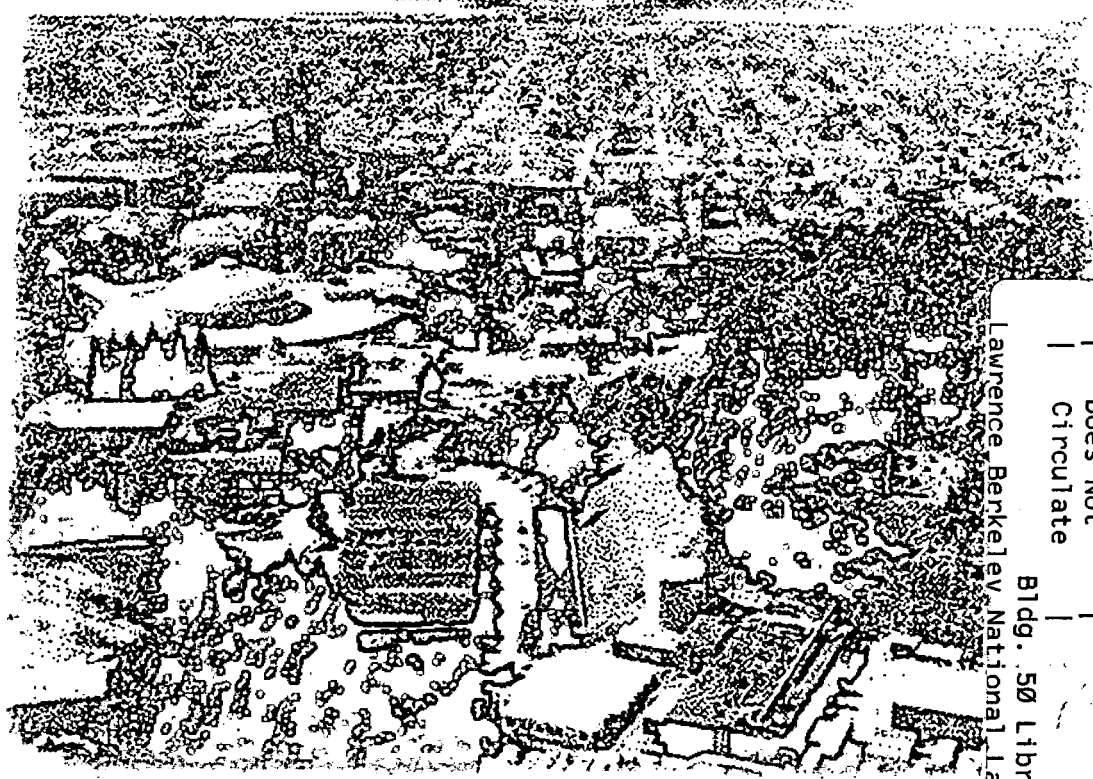

REFERENCE COPY
Does Not
Circulate
Bldg. 50 Library - Ref.
Lawrence Berkeley National Laboratory
LBNL-41558
Copy 1

DISCLAIMER

This document was prepared as an account of work sponsored by the United States Government. While this document is believed to contain correct information, neither the United States Government nor any agency thereof, nor the Regents of the University of California, nor any of their employees, makes any warranty, express or implied, or assumes any legal responsibility for the accuracy, completeness, or usefulness of any information, apparatus, product, or process disclosed, or represents that its use would not infringe privately owned rights. Reference herein to any specific commercial product, process, or service by its trade name, trademark, manufacturer, or otherwise, does not necessarily constitute or imply its endorsement, recommendation, or favoring by the United States Government or any agency thereof, or the Regents of the University of California. The views and opinions of authors expressed herein do not necessarily state or reflect those of the United States Government or any agency thereof or the Regents of the University of California.

LBNL-41558

THE INTENSIFICATION OF TWO-DIMENSIONAL SWIRLING FLOWS BY STOCHASTIC ASYMMETRIC FORCING[1]

David S. Nolan[2]

Mathematics Department
Computing Sciences Directorate
Lawrence Berkeley National Laboratory
Berkeley, CA 94720

Brian F. Farrell
Department of Earth and Planetary Sciences
Harvard University
Cambridge, MA 02138

Submitted to *Journal of the Atmospheric Sciences*

March 12, 1998

[1]This work was supported in part by the Applied Mathematical Sciences Subprogram of the Office of Energy Research, U.S. Department of Energy, under Contract DE-AC03-76SF00098.

[2]Corresponding author address: 50A-2152, Lawrence Berkeley National Laboratory, 1 Cyclotron Road, Berkeley, CA 94720; *nolan@math.lbl.gov*

Abstract

We investigate the effects of stochastically excited asymmetric disturbances on two-dimensional vortices. These vortices are maintained by the radial inflow of fixed cylindrical deformation fields, which are chosen so that both one-celled and two-celled vortices may be studied. We reduce the linearized perturbation equations to the form of a linear dynamical system with stochastic forcing, i.e., $d\mathbf{x}/dt = \mathbf{A}\mathbf{x} + \mathbf{F}\xi$, where the columns of $\mathbf{F}$ are forcing functions and the elements of ξ are gaussian white-noise processes. Through this formulation we can directly calculate the stochastically maintained variance of the perturbations, the structures that dominate the response (the empirical orthogonal functions), and the forcing functions that contribute most to this response (the stochastic optimals).

We find that for all cases the structures that dominate the transfer of energy from the mean flow to the perturbation field are close approximations to the global optimals, and that the structures which account for most of the variance are close approximations to the the global optimals evolved forward in time to when they reach their maximum energy. For azimuthal wavenumbers in each vortex where nearly-neutral modes are present (k=1 for the one-celled vortex and $1 \leq k \leq 4$ for the two-celled vortex) the variance sustained by the stochastic forcing is large, and in these cases we show that this variance may be greatly overestimated if the radial inflow that sustains the mean vortex is neglected in the dynamics of the perturbations.

Through a modification of our technique we can also find the ensemble average eddy momentum flux divergences associated with the stochastically maintained perturbation fields, and we use this information to determine the perturbation induced mean flow tendency in the linear

limit. Examination of these results shows that the net effect of the perturbations is to cause downgradient eddy fluxes for low wavenumbers in both vortex types, and to cause upgradient eddy fluxes for high wavenumbers. However, to determine how these eddy fluxes will actually change the mean flow, we must incorporate the local accelerations caused by the eddy flux diveregnces into the equation for the steady-state azimuthal velocity field to determine the deviation of the mean (symmetric) flow. From calculations of this type we find that the effect of the radial inflow can be crucial in determining whether or not the vortex is intensified or weakened by the perturbations: though the net eddy fluxes are most often downgradient, the radial inflow carries the transported angular momentum back into the vortex core, resulting in an increase in the maximum windspeed. Thus we find that in most cases for the vortex flows we have studied, the net effect of stochastically forced asymmetric perturbations is to intensify the mean vortex.

1 Introduction

In recent years the dynamics of asymmetric disturbances in effectively two-dimensional swirling flows has been studied extensively due to their role in understanding phenomena in intense atmospheric vortices such as hurricanes and tornadoes. Some of these applications to hurricane dynamics are the following: asymmetric disturbances to the storm potential vorticity field has been advanced as an explanation for the appearance of spiral rainbands (Guinn and Schubert, 1993; Montgomery and Kallenbach, 1997), in contrast to the earlier gravity-wave theories (Kurihara, 1976); asymmetric dynamics is used to explain both long-and short-term deviations of the hurricane track from that prescribed by the surrounding flow (Willoughby, 1992, 1994; Smith and Weber, 1993); and the rapid decay of higher-wavenumber disturbances in the vicinity of the vortex core helps explain the robustness of these storms to adverse influences such as the beta effect and the shear of the environmental wind (Carr and Williams, 1989; Smith and Montgomery, 1995).

Asymmetric dynamics has long been of interest in the study of tornadoes since the realization that tornadoes sometimes contain several smaller vortices within the larger vortex core, and that the greatest damage is often found in the paths of these smaller vortices (Fuijita, 1971). This phenomenon has been widely reproduced in both laboratory (Ward, 1972; Church, et al., 1979) and numerical models (Rotunno, 1984; Lewellen, 1993; Lewellen, et al., 1997). Instability of the vertical and azimuthal velocity field in the core of the tornado has been offered as an explanation for the appearance of "multiple vortices" in numerous reports addressing the linear stability of inviscid swirling flows (Rotunno, 1978; Staley and Gall, 1979, 1984; Steffens, 1988) and similar

flows with viscosity (Staley, 1985). The general result has been to find instability for a finite range of low wavenumbers for two-dimensional instabilities, and a larger range of higher-wavenumber instabilities for three-dimensional (spiral) structures which are identified as inertial instabilities (Leibovich and Stewartson, 1983; Emanuel, 1984). Interest in asymmetric tornado dynamics has been renewed by the discovery that three-dimensional models can sustain realistic tornado wind-speeds (Lewellen, et al., 1997; Fiedler, 1998) while in the past axisymmetric models have not (Fiedler, 1993, 1994; Nolan and Farrell, 1998b). The higher windspeeds of the three-dimensional models have been associated with the simulated multiple vortices that appear in them, as Fujita (1971) himself anticipated for actual tornadoes.

A feature common to virtually all previous studies of vortex dynamics and stability has been neglect of the radial inflow which must be present to sustain the mean vortex flow against the effects of dissipation. This omission is due to the additional analytical difficulties brought on by the effects of radial advection on the perturbations and the fact that the presence of radial mean velocities makes the problem inherently three dimensional in most cases, i.e., not susceptible to analysis with perturbations of the usual form $F(r)e^{i(k\theta + mz + \omega t)}$. Nolan and Farrell (1998a) were able to overcome these obstacles by constructing mean vortex flows with radial inflow for which initially two-dimensional perturbations remained strictly two-dimensional, and then by allowing the radial structure function of the perturbations to vary both temporally and radially. Two kinds of two-dimensional vortex flows were examined: one-celled vortices, where radial inflow penetrates all the way to the axis and the vortex core is in solid-body rotation, and two-celled vortices, where the radial inflow does not penetrate to the axis and the vortex core is stagnant. A change in sign of the mean-flow vorticity gradient in the two-celled vortex allows for modal instability in the range of azimuthal wavenumbers $3 \leq k \leq 10$, while the one-celled vortex was found to be stable

for all wavenumbers. Furthermore, with the use of generalized stability theory (Farrell and Ioannou, 1996) it was found that for both vortex types there could also be substantial transient growth in energy of optimally configured initial perturbations. Neglect of the dynamical terms associated with the radial inflow that sustains the mean vortex - the radial advection and the stretching terms - was shown to result in a large overestimate of the potential for transient growth in the one-celled vortex and also to destabilize azimuthal wavenumbers one and two in the two-celled vortex.

Nolan and Farrell (1998a) also investigated whether or not the eddy momentum fluxes associated with transiently growing disturbances cause a net tendency toward increase or decrease in the maximum windspeed of the mean vortex. While in most cases the net effect of introducing a disturbance is to increase the kinetic energy of the mean flow, the opposite result can be found in both one- and two-celled vortices for wavenumbers that have nearly-neutral modes. In these cases, energy acquired from the mean flow during the growth stage of the disturbance was trapped in these nearly-neutral modes and ultimately lost to dissipation, rather than being returned to the mean flow. This effect was previously discussed by Smith and Montgomery (1995) in an analysis of evolving perturbations in an unbounded Rankine vortex, although they did not discuss the resulting effect on the mean flow.

Transient growth of asymmetric disturbances in a vortex is a close analog to the transient growth phenomenon in linear shear flows originally demonstrated by Kelvin (1887) and Orr (1907). This analogy has been further elucidated in discussions and examples by Smith and Montgomery (1995), Kallenbach and Montgomery (1995), and Nolan (1996). While the potential for susbtantial transient growth of properly configured initial disturbances certainly exists, Montgomery and Kallenbach (1997) have argued it is exceedingly unlikely to occur since the typical optimal initial condition for growth is a disturbance that is a tight, reverse sprial in the opposite

direction of the flow, and there is no apparent mechanism to excite such disturbances in atmospheric vortices. Our work here will address this issue to some extent by exciting asymmetric perturbations in our mean vortex flows with forcing functions that are unbiased is space and time, so that we will answer the question: what role do these transiently growing disturbances play when the forcing lacks the bias of a preferred spatial structure? While this analysis does not necessarily apply to atmospheric vortices where only certain types of disturbances may be introduced, it will lend considerable insight into the importance of including both radial inflow and transient growth in the analysis of asymmetric vortex dynamics.

Section 2 gives an introduction to the analysis of linear dynamical systems when they are excited by a stochastic forcing term. Section 3 will describe the two-dimensional vortex flows under consideration and give a brief description of how the evolution governing perturbations to this flow can be reduced to the form $d\mathbf{x}_k/dt = \mathbf{A}_k\mathbf{x}_k$ for each azimuthal wavenumber k. Section 4 describes the response of the vortices to the stochastic forcing, and Section 5 investigates how this response feeds back onto the mean flow of the vortex through eddy momentum fluxes. Discussion of some of the important points are provided in Section 6, and conclusions are presented in Section 7.

2 Stochastically Driven Linear Dynamical Systems

An introduction to the theory of stochastic differential equations can be found in Gardiner (1985). Particular results for white-noise forcing have already been applied to the study of non-normal shear flows, as discussed above, by Farrell and Ioannou (1993, 1994), DelSole (1993), and DelSole and Farrell (1996). In the following paragraphs we follow the approach of these authors to solve directly for the response of a linear dynamical system driven by stochastic forcing with

white noise properties.

We begin by assuming our perturbation evolution equations have been reduced to a non-normal linear dynamical system in generalized velocity coordinates [defined below in (3.22) and (3.23); for examples of this process see Farrell and Ioannou, 1993c; Delsole and Farrell, 1996; Nolan and Farrell (1998a)]. Now we add to the system a random forcing term $\mathbf{F}\xi$:

$$\frac{d\mathbf{x}}{dt} = \mathbf{A}\mathbf{x} + \mathbf{F}\xi \tag{2.1}$$

The columns of the matrix operator $\mathbf{F}$ are a set of forcing functions, each separately driven randomly by the elements of the vector $\xi(t)$. The elements of $\xi(t)$ are complex Gaussian white-noise processes, having zero mean and unit covariance:

$$\langle \xi_i(t) \rangle = 0 \tag{2.2}$$

$$\langle \xi_i(t_1)\xi_j^*(t_2) \rangle = \delta_{ij}\delta(t_1 - t_2) \tag{2.3}$$

where the brackets refer to ensemble averages, and δ_{ij} is the Kronecker delta. The solution in time to (2.1) is:

$$\mathbf{x}(t) = e^{\mathbf{A}t}\mathbf{x}(0) + \int_0^t e^{\mathbf{A}(t-s)}\mathbf{F}\xi ds \tag{2.4}$$

The first term on the RHS of (2.4) refers to the evolution of the initial conditions, which decay to zero when all the eigenvalues of $\mathbf{A}$ have negative real part. Since this is true for all of the systems considered here we can ignore this term in subsequent analyses which focus on steady states achieved as $t \rightarrow \infty$. The second term is the accumulated effect of all of the forcings from $t=0$ to the present time t.

Recalling that in the generalized velocity coordinates the energy of the system $E = \mathbf{x}^*\mathbf{x}$, one can directly solve for the ensemble average energy of the perturbations as a function of time:

$$\begin{aligned}\langle E^t\rangle &= \langle \mathbf{x}^*(t)\mathbf{x}(t)\rangle \\ &= \langle \int_0^t ds \int_0^t \xi^* \mathbf{F}^\dagger e^{\mathbf{A}^\dagger(t-s)} e^{\mathbf{A}(t-s)} \mathbf{F}\xi ds\rangle \\ &= \mathbf{F}^\dagger\left(\int_0^t e^{\mathbf{A}^\dagger(t-s)} e^{\mathbf{A}(t-s)} ds\right)\mathbf{F} \\ &= \mathrm{Trace}[\mathbf{F}^\dagger \mathbf{B}^t \mathbf{F}]\end{aligned} \tag{2.5}$$

where we have made use of the properties (2.2) and (2.3) of the forcing terms, and defined the Hermitian operator $\mathbf{B}^t$ as:

$$\mathbf{B}^t = \int_0^t e^{\mathbf{A}^\dagger(t-s)} e^{\mathbf{A}(t-s)} ds \tag{2.6}$$

Thus we can see that the energy of the system depends both on the dynamics of the system as represented in A and on the structures and magnitudes of the forcing functions in **F**. It can also be seen that an eigenvalue decompostion of $\mathbf{B}^t$ will provide a set of functions ordered in the extent to which they would excite the system at time t as forcing functions, with their relative responses described by their positive definite eigenvalues. These forcings are referred to as "stochastic optimals" (hereafter SOs).

With some manipulation we can solve for the steady state solution of (2.5). Differentiating (2.6) with respect to the time t, we find a time evolution equation for $\mathbf{B}^t$:

$$\frac{d\mathbf{B}^t}{dt} = \mathbf{I} + \mathbf{A}^\dagger \mathbf{B}^t + \mathbf{B}^t \mathbf{A} \tag{2.7}$$

where **I** is the identity matrix. We would like to find $\mathbf{B}^\infty$ without having to directly evaluate $\lim_{t\to\infty} \mathbf{B}^t$. Since all the eigenvalues of **A** have negative real part, as $t \to \infty$ the system achieves a statistically steady state and the time rate of change must go to zero, so:

$$\mathbf{A}^{\dagger}\mathbf{B}^{\infty} + \mathbf{B}^{\infty}\mathbf{A} = -\mathbf{I} \tag{2.8}$$

An equation of this form is known as a Lyapunov equation, and can be solved by standard methods (Lefschetz, 1963; DelSole, 1993). Eigenvector decomposition of $\mathbf{B}^{\infty}$ provides the SOs for the system when it has reached a steady state.

Through a very similar procedure we can find the structures that represent an ordered decomposition of the response of the system to the stochastic forcing, usually referred to as empirical orthogonal functions (EOFs). To find the EOFs, we need the full correlation matrix of the system:

$$\begin{aligned} \mathbf{C}_{ij}^{t} &= \langle \mathbf{x}_i(t)\mathbf{x}_j^*(t)\rangle \\ &= \langle \int_0^t ds \int_0^t e^{\mathbf{A}(t-s)}\mathbf{F}\xi\xi^*\mathbf{F}^{\dagger}e^{\mathbf{A}^{\dagger}(t-s)}ds\rangle \\ &= \left(\int_0^t e^{\mathbf{A}(t-s)}\mathbf{H}e^{\mathbf{A}^{\dagger}(t-s)}ds\right)_{ij} \end{aligned} \tag{2.9}$$

where we have written $\mathbf{H} = \mathbf{F}\mathbf{F}^{\dagger}$. When $\mathbf{F}$ is unitary $\mathbf{H} = \mathbf{I}$; therefore all unitary forcing operators result in the same response. By differentiating (2.9) we obtain an evolution equation for the correlation matrix:

$$\frac{d\mathbf{C}^t}{dt} = \mathbf{H} + \mathbf{A}\mathbf{C}^t + \mathbf{C}^t\mathbf{A}^{\dagger} \tag{2.10}$$

and we can also find the steady state solution in terms of a Lyapunov equation:

$$\mathbf{A}\mathbf{C}^{\infty} + \mathbf{C}^{\infty}\mathbf{A}^{\dagger} = -\mathbf{H} \tag{2.11}$$

The decompostion of the full correlation matrix (2.9) into its orthogonal eigenfunctions is known as the Karhunen-Loeve (K-L hereafter) decomposition (Loeve, 1978), while the decomposition of the space of forcing functions into orthogonal functions ordered by their contribution to the variance has been called the "back K-L decomposition" by Farrell and Ioannou (1993c).

Observe that when the forcing is unitary so that $\mathbf{H} = \mathbf{I}$ the equations (2.8) and (2.11) for the SOs and the EOFs have a certain antisymmetry. On the other hand, when the dynamical operator $\mathbf{A}$ is normal the eigenfunctions of both $\mathbf{B}^{\infty}$ and $\mathbf{C}^{\infty}$ reduce to the complete and orthogonal eigenfunctions of $\mathbf{A}$. In this case the response of the system can be entirely predicted and interpreted in terms of these eigenfunctions, or normal modes, of $\mathbf{A}$. (In fact, each normal mode would behave like a stochastically forced damped harmonic oscillator, independently of the other modes). When $\mathbf{A}$ is not normal, as in the case of our vortex flows, the forcing functions and response functions differ in a manner similar to the least damped modes and the least damped modes of the adjoint operator $\mathbf{A}^{\dagger}$ (for examples, see Farrell, 1988; DelSole and Farrell, 1996; or Nolan and Farrell, 1998a). The fact that the EOFs of a non-normal system are distinct from the modes of the dynamical operator has been addressed and discussed by North (1984).

Finally, we note that the average perturbation energy can be found from both the forcing matrix and the response matrix:

$$E^{\infty} = \mathrm{Trace}\{\mathbf{C}^{\infty}\} = \mathrm{Trace}\{\mathbf{F}^{\dagger}\mathbf{B}^{\infty}\mathbf{F}\} \tag{2.12}$$

while the energy input from the stochastic forcing is:

$$E_{in} = \mathrm{Trace}(\mathbf{F}^{\dagger}\mathbf{F}) = N \tag{2.13}$$

when $\mathbf{F}$ is unitary and has rank N.

3 Two Steady-State Vortex Flows and Equations for the Evolution of Asymmetric Perturbations

In this section we briefly describe the one- and two-celled vortices whose dynamics we are going to study. We also derive equations of motion for two-dimensional, asymmetric perturbations and reduce them to the form of a linear dynamical system $d\mathbf{x}/dt = \mathbf{A}\mathbf{x}$. For more details

and discussion see Nolan and Farrell (1998a).

3.1 The one-celled vortex

We wish to find a steady-state solution for the azimuthal velocity field sustained by a fixed cylindrical deformation field, which is analogous to the Burgers' vortex solution (Burgers, 1948; Rott, 1954) but is contained in a closed domain. We define a cylindrically symmetric radial velocity function that is fixed in time:

$$U = U(r) \tag{3.1}$$

By continuity, we have:

$$\frac{\partial W}{\partial z} = -\frac{1}{r}\frac{\partial}{\partial r}(rU) \tag{3.2}$$

so that the vertical velocity field $W(r, z)$ may be determined up to constant. Holding the U and W velocities fixed, we can write down a single advection-diffusion equation for the evolution of the axisymmetric azimuthal velocity $V(r)$:

$$\frac{\partial V}{\partial t} + U\frac{\partial V}{\partial r} + \frac{UV}{r} = \nu\left(\frac{\partial^2 V}{\partial r^2} + \frac{1}{r}\frac{\partial V}{\partial r} - \frac{V}{r^2}\right) \tag{3.3}$$

We use a cylindrically symmetric deformation field similar to the Burgers' vortex deformation field, except that its support lies entirely within a cylinder of radius r=b=7. Furthermore, we require that the radial inflow velocity transitions very smoothly to zero as we approach the outer boundary, and is nearly zero for a substantial region near the outer boundary. Such a radial inflow function is given by:

$$U(r) = -\alpha r e^{-\mu r^6} \tag{3.4}$$

This function with $\alpha = 5.0 \times 10^{-3}$ and $\mu = 2.44 \times 10^{-4}$ is shown in Figure 1a. This particular choice for α, in conjunction with a choice of ν=0.001 for the viscosity, sets the radius of maxi-

mum winds r_{max}=1 for the well-known Burgers' vortex solution (see Burgers, 1948 or Rott, 1954). Using this radial velocity field and an outer boundary condition on V such that the circulation at the outer boundary $\Gamma_b = 2\pi r_b V_b = 2\pi$ (i.e., the circulation of the fluid at the edge of the domain is equal to 2π everywhere), (3.3) results in the solution shown in Figure 1b. The *vortex Reynolds number*, as it is usually defined, is $Re_V = r_b V_b/\nu = 1000$. This solution, which has r_{max}=1.0 and maximum azimuthal windspeed v_{max}=0.71, is virtually identical to the Burgers' solution with the same parameters, despite the fact that the radial inflow velocity transitions to zero near the outer edge of the domain. The deformation (or negative horizontal divergence) of the radial velocity function is shown in Figure 1c, while the radial gradient of the vertical component of vorticity is shown in Figure 1d.

3.2 Two-celled vortices

A simple model of a two-celled vortex is created by defining the radial velocity $U(r)$ to have inflow outside some radius, and outflow away from the r=0 axis, with a stagnation point in between:

$$U(r) = \begin{cases} 0 & r < 0.2 \\ 0.02\sin^2\left(\pi\frac{r-0.2}{1.6}\right) & 0.2 < r < 1 \\ 0.035\cos\left(\pi\frac{r-1}{2.0}\right) - 0.15 & 1 < r < 3 \\ -0.05\cos^2\left(\pi\frac{r-3}{7.0}\right) & 3 < r < 6.5 \\ 0 & r > 6.5 \end{cases} \tag{3.5}$$

This radial velocity function is shown in Figure 2a. In previous work, Nolan and Farrell (1998a) used this radial velocity field and a viscosity of ν=0.001 to produce a two-celled vortex with a completely stagnant core ($V \cong 0$ for r<1.2); however, that vortex is unstable for azimuthal wave-

numbers $3 \le k \le 10$. Since we cannot study the stationary statistics of a linear dynamical system with an unstable operator **A**, we instead increase the viscosity until the vortex is marginally stable for all wavenumbers; this has the side effect of smoothing the resultant azimuthal velocity field so that it is non-zero in the vortex core. The smallest viscosity that stabilizes this two-celled vortex for all azimuthal wavenumbers was found to be ν=0.0058. Applying our method with this higher viscosity, where again we have defined the circulation at the outer boundary $\Gamma_b = 2\pi$, we find the azimuthal velocity profile shown in Figure 2b. In this case r_{max}=2.19, and v_{max}=0.43. The associated deformation function is shown in Figure 2c, while the resulting vertical vorticity gradient is shown in Figure 2d. Outside r_{max} the velocity profile is nearly that of a potential flow. A stability diagram for this modified two-celled vortex is shown in Figure 3, along with the stability curve for an identical azimuthal velocity profile with the radial inflow terms neglected in the perturbation dynamics. Neglect of the radial inflow which sustains the mean vortex circulation nearly destabilizes the two-celled vortex for azimuthal wavenumber k=1 (decay rate $1.1\text{x}10^{-4}$), and does destabilize the vortex for k=2 and k=3.

3.3 The evolution of vertical vorticity perturbations

We restrict our attention to the dynamics of the vertical vorticity component ζ, in cylindrical coordinates. This vertical vorticity component is assumed to have no variation in the vertical direction and its dynamics are governed by:

$$\frac{\partial \zeta}{\partial t} + u\frac{\partial \zeta}{\partial r} + \frac{v}{r}\frac{\partial \zeta}{\partial \theta} = \zeta\frac{\partial w}{\partial z} + \nu\left[\frac{\partial^2 \zeta}{\partial r} + \frac{1}{r}\frac{\partial \zeta}{\partial r} + \frac{1}{r^2}\frac{\partial^2 \zeta}{\partial \theta}\right] \tag{3.6}$$

Now, we write each term in (3.6) as the sum of a radially varying mean and azimuthally, radially, and temporally varying perturbations: $u = U(r) + u'(r, \theta, t)$, $\zeta = Z(r) + \zeta'(r, \theta, t)$, and similarly for v and w. We can then separate the solutions by writing them as a sum of harmoni-

cally varying azimuthal waves, i.e., $\zeta'(r, \theta, t) = \sum_k \zeta_k(r, t)e^{ik\theta}$, and so on for the perturbations of u and v also. Substituting these forms into (3.6), we obtain for each wavenumber k a linear equation for the evolution of the radially and temporally varying vorticity function $\zeta_k(r, t)$:

$$\left(\frac{\partial}{\partial t} + U(r)\frac{\partial}{\partial r} + ik\Omega(r)\right)\zeta_k + u_k\frac{\partial Z}{\partial r} = \zeta_k\frac{\partial W}{\partial z} + \nu\left[\frac{\partial^2\zeta_k}{\partial r^2} + \frac{1}{r}\frac{\partial\zeta_k}{\partial r} - \frac{k^2}{r^2}\zeta_k\right] \tag{3.7}$$

From here on we will use the convention that the terms u_k, v_k, ζ_k refer to complex amplitude functions of r and t only.

As we can see from (3.7), when there is a non-zero background vorticity gradient $\partial Z/\partial r$, obtaining the evolution of the perturbation vorticity requires knowledge of the radial velocity perturbations. Following Carr and Williams (1989) and Smith and Montgomery (1995), we find the velocities by solving for the perturbation streamfunction:

$$\psi(r, \theta, t) = \sum_k \psi_k(r, t)e^{ik\theta} \tag{3.8}$$

$$u_k = \frac{-1}{r}\frac{\partial\psi_k}{\partial\theta} = \frac{-ik}{r}\psi_k \tag{3.9}$$

$$v_k = \frac{\partial\psi_k}{\partial r} \tag{3.10}$$

We choose as boundary conditions no normal flow at the outer boundary $r=b$, i.e.:

$$\psi_k(0, t) = \psi_k(b, t) = 0 \tag{3.11}$$

Given the vorticity, the streamfunction may be found with a Green's function:

$$\psi_k(r, t) = \int_a^b G_k(r, \rho)\zeta_k(\rho, t)d\rho \tag{3.12}$$

The Green's function appropriate for this problem is

$$G_k(r,\rho) = \begin{cases} \dfrac{r^{2k}}{2kr^k b^{2k}}(\rho^{k+1} - b^{2k}\rho^{-k+1}) & 0 \le r \le \rho \\ \dfrac{r^{2k} - b^{2k}}{2kr^k b^{2k}}\rho^{k+1} & \rho \le r \le b \end{cases} \tag{3.13}$$

[see Carr and Williams (1989), with the inner boundary a set to zero].

3.4 Reduction to a linear dynamical system in generalized velocity coordinates

We would like to find the linear dynamical system in matrix form which governs the evolution of the perturbations. We discretize the domain by assigning the values of the radial functions to evenly spaced points from $r = 0 + \Delta r$ to $r = b - \Delta r$, each point separated by a distance Δr. This converts the continuous radial functions into vectors of length $N = (b/\Delta r) - 1$. For all calculation spresented here we use Δr=0.5 so that N=139. We express all derivatives as matrix operators corresponding to the usual centered-difference approximations, with the exception that the finite difference operator used for the advection term is one-sided, representing a second-order upwinding advection scheme. We must also express the Green's function operation (3.12) as a matrix operation, i.e.:

$$\psi_k = \mathbf{G}_k \zeta_k \tag{3.14}$$

Finally, the vorticity evolution equation (3.7) is put in matrix dynamical system form with only the time derivative on the L.H.S.:

$$\frac{d\zeta_k}{dt} = \mathbf{T}_k \zeta_k \tag{3.15}$$

with:

$$\mathbf{T}_k = -\mathbf{U}\mathbf{D}_{up} - ik\Omega + (\mathbf{D}\mathbf{Z})ik\mathbf{R}^{-1}\mathbf{G}_k + \mathbf{S} + \nu(\mathbf{D}^2 + \mathbf{R}^{-1}\mathbf{D} - k^2\mathbf{R}^{-2}) \tag{3.16}$$

Where we have written $\mathbf{D}$ for the matrix representing the finite-difference derivative with respect to r, $\mathbf{D}_{up}$ for a similar but upwinded deriviative operator, $\mathbf{R}$ for the radius, and $\mathbf{S}$ for the "stretching" term $\partial W/\partial z$. We must also incorporate into these difference operators additional boundary conditions on the vorticity, which we choose to be:

$$\zeta_k(0) = \zeta_k(b) = 0 \tag{3.17}$$

This condition minimizes the effects of the outer boundaries on the interior dynamics.

The kinetic energy of each perturbation is:

$$E = \int_0^b \left(\frac{\overline{u_k^2}}{2} + \frac{\overline{v_k^2}}{2}\right) 2\pi r dr = -\frac{1}{2}\int_0^b \overline{\psi_k \zeta_k} 2\pi r dr = -\frac{\pi}{4}\int_0^b (\psi_k{}^* \zeta_k + \zeta_k{}^* \psi_k) r dr \tag{3.18}$$

where the overbars refer to azimuthal averages of the real parts of the complex functions. We define an energy metric operator $\mathbf{M}$ such that the energy of our discretized linear dynamical system is written $E = \zeta^* \mathbf{M} \zeta$. For each azimuthal wavenumber k the energy metric can be formulated from (3.18)

$$\mathbf{M}_k = \frac{-\pi\Delta r}{4}[\mathbf{G}_k{}^\dagger \mathbf{R} + \mathbf{R}\mathbf{G}_k]. \tag{3.19}$$

By the additional transformations:

$$\mathbf{x}_k = \mathbf{M}_k^{1/2} \zeta_k \tag{3.20}$$

$$\mathbf{A}_k = \mathbf{M}_k^{1/2} \mathbf{T}_k \mathbf{M}_k^{-1/2} \tag{3.21}$$

the system is converted into *generalized velocity coordinates*, so that the dynamics are expressed in the canonical form:

$$\frac{d\mathbf{x}_k}{dt} = \mathbf{A}_k\mathbf{x}_k \tag{3.22}$$

$$E = \mathbf{x}_k{}^*\mathbf{x}_k \tag{3.23}$$

4 Stochastic Forcing of Inflow-Driven Vortices: System Response

In this section we will use the techniques described in section 2 to solve directly for the variance of stochastically driven perturbations in our one- and two-celled vortices. We will also use the K-L decomposition and back K-L decomposition to find the structures that contain most of the variance (the EOFs), and also the forcing functions that result in the most variance (the SOs). The effect of inflow velocity on the variance is also shown.

4.1 Response to stochastic forcing of the one-celled vortex

Figure 4 shows contour plots of the vorticity and streamfunction fields of the primary SOs for k=1 and k=2 in the one-celled vortex, which contribute 66% of the variance and 24% of the variance, respectively. These perturbations are fairly similar and have two important features: first, they are structures that spiral back against the flow of the vortex, and second, they are displaced from the core of the vortex, with their maximum vorticities and streamfunctions near r=5. These two features are indicative of how a perturbation must be initially configured so as to maximize the energy it acquires from the mean flow, as has previously been demonstrated by Nolan and Farrell (1998a) for vortex flows with radial inflow. Such perturbations must spiral back against the vortex flow so that they are everywhere locally tilted back against the shear of the mean flow, and they must lie outside the vortex core so that they will be not be swept into the vortex core before they can maximize their wave-mean flow interactions.

This point emphasized by comparison with Figure 6ab which shows the vorticity and

streamfunction fields for the k=1 global optimal for the one-celled vortex. The global optimal is the perturbation that grows the most in energy (in this case, by a factor of 181), and its growth is one measure of the potential for wave-mean flow interaction in a particular mean flow. The strong similarity between the stochastic optimal and the global optimal shows that the extent to which stochastic forcing excites transient growth of perturbations is closely related in this example to the extent to which the forcing projects onto the global optimals.

We can also find the dominant perturbations structures that result from the stochastic forcing as described above in section 2. This system response depends on the structure of the forcing functions in the columns of the matrix **F**, as shown in (2.9), but it is the same for all unitary **F**. When **F** is unitary we are forcing all scales equally in energy. Using such a unitary set of forcing functions and normalizing the rate of energy input to one [see (2.13)], Figure 5 shows the primary EOFs for k=1 and k=2 in the one-celled vortex, which represent 98% and 43% of the variance, respectively. For the same reasons that the primary SOs were very similar to the global optimals, these structures are very similar to the *realizations* of the global optimals which are shown in Figure 6cd. The realizations of the global optimals are the structures that the global optimals become when they obtain their maximum energy as they are deformed by the mean flow. This maximum energy is achieved when the vorticity has been arranged into the most coherent structure possible, an arrangement which maximizes its associated flow field and therefore its kinetic energy. The strong similarity betwen the EOFs and the realizations of the global optimals again emphasizes that the transfer of energy from the mean flow to perturbations is dominated by excitation of the global optimals. Furthermore, the fact that the k=1 primary EOF represents so much (98%) of the variance is caused by the close similarity between the realization of the global optimal and the least damped mode [see Nolan and Farrell (1998a)]; when growing structures reach their maxi-

mum energy, their energy is trapped in the nearly-neutral least damped mode, which in this case has a decay rate of 2.0×10^{-3}. For higher wavemumbers the realiztions of the global optimals and the least damped modes are not similar in structure.

4.2 Response to stochastic forcing of the two-celled vortex

Figure 7 shows the primary SOs for k=1 and k=3 in the two-celled vortex, which represent 61% and 98% of the contribution to the variance, respectively. These structures are very similar to the SOs for the one-celled vortex, with the exception that they have vorticity in the vortex core, due to the fact that voriticity is being advected outward from the center axis as well as inward from the outer boundary. We again see the similarity between the SOs and the global optimals, shown for k=3 in the two-celled vortex in Figure 9ab. Note however that in this case of the two-celled vortex, both the realizations of the global optimals and the EOFs for this wavenumber are not like the symmetric, coherent structures that we saw above for the one-celled vortex, but rather they are very close approximations to the least-damped modes (not shown), which are structures that sustain themselves by converting mean-flow vorticity to perturbation vorticity. Thus, instead of being sheared over by the mean flow, the global optimal evolves into a nearly-neutral structure that persists for long times. Further discussion of this point may be found in Nolan and Farrell (1998a).

The primary EOFs for k=1 and k=3 in the two-celled vortex, as shown in Figure 8, represent 76% and 98% of the variance under unitary stochastic forcing. They again have structures similar to the realizations of the global optimals, which are shown for k=3 in Figure 9cd. Therefore we conclude that the wave-mean flow interactions are dominated by the excitation of the global optimals in the two-celled vortex as well.

4.3 Sustained variance and the effects of radial inflow

The total varianced sustained by the stochastic forcing of the system can be be found as in

(2.12). In flows with strong shear, this variance greatly exceeds that estimated by equating the energy input to the modal dissipation which, assuming all modes are stable and equally excited (as in the case of unitary sets of forcing functions **F**), would be:

$$E^{\infty}_{modal} = \frac{1}{N}\sum_{i=1}^{N}\frac{1}{(\lambda_i + \lambda_i^*)} \tag{4.1}$$

where the λ_i are the eigenvalues of **A**, N is the dimension of the system, and the rate of energy input has been normalized to be equal to one. Such a calculation is correct for a dynamical system with a normal operator **A** (such as a set of damped harmonic oscillators), but it is incorrect for non-normal systems such as those representing fluid flows with shear. In this case the sustained variance is usually much greater than that computed from (4.1), and in fact Iouannou (1995) showed rigorously that the correctly computed variance (2.12) is always greater than that estimated from the dissipation rates of the modes:

$$E^{\infty} = \mathrm{Trace}[\mathbf{C}^{\infty}] \geq E^{\infty}_{modal} \tag{4.2}$$

with the equality occurring only when **A** is normal. The increased variance in shear flows such as ours is due to transiently growing disturbances which acquire energy from the mean flow.

Figure 10 shows the variance under stochastic forcing functions that are unitary (and normalized to one unit of energy input per unit time) as a function of azimuthal wavenumber in the one- and two-vortices. For each vortex we have plotted the variance in three different cases: 1) the variance computed from (4.2); 2) this same variance but with the radial inflow terms [**S** and -$\mathbf{UD}_{up}$ in (3.16)] neglected in the perturbation dynamics; and 3) the variance of an "equivalent normal" system, i.e., that calculated from (4.1). For both vortices the actual variance is about an order of magnitude larger than the equivalent normal variance at all wavenumbers. Secondly, with the exceptions of k=4 and k=5 for the two-celled vortex, in all cases the variance is larger when

the radial inflow is neglected, although only by a small percentage for $k>1$ in the one-celled vortex and $k>5$ in the two-celled vortex.

We now wish to further evaluate the impact of radial inflow on the variance. We will do this in two steps: for each vortex, we will vary the relative magnitude of the radial inflow field over a range of values from half its original strength to twice its original strength. Then, for each value of the strength of the radial inflow, we first recalculate the resultant steady-state azimuthal velocity field. For stronger radial inflow fields, the vortex will be tighter and more intense; for weaker radial inflow the vortex will be broader and weaker. Then, we will calculate the sustained variance of the perturbations, *and* the same variance with the dynamical terms associated with radial inflow (the advection and stretching) eliminated. For each case we also show the variance of an equivalent normal system. The results for $k=1$ and $k=2$ in the one-celled vortex are shown in Figure 11. For $k=1$, we have a remarkable result: the variance of the wavenumber one perturbations is over two orders of magnitude less in the presence of radial inflow than without it. The variance with the radial inflow included is itself about two orders of magnitude larger than the variance of an equivalent-normal system (with inflow). For $k=2$, the variances with and without inflow are nearly equal, but we also see that the variance declines as the strength of the radial inflow is increased, and that both of these are ten times larger than the equivalent normal variance.

The results for $k=1$ in the two-celled vortex are shown in Figure 12a. Again, the variance is much larger than that of an equivalent-normal system, and the variance declines with increasing radial inflow. Results for $k=8$, shown in Figure 12b, are quite similar to the $k=2$ (and for all higher wavenumbers) case for the one-celled vortex shown in Figure 11b: the variance is only slightly suppressed by radial inflow and the magnitude of the variance itself is very small as compared to the energy input per unit time, which has been normalized to one.

5 Momentum Fluxes and Mean Flow Deviations

We have established that stochastic excitation of asymmetric disturbances in the vortices we are studying leads to excitation of transiently growing perturbations that contribute greatly to the sustained perturbation variance, and that the effect of including the dynamically consistent radial inflow that sustains the mean flow is to suppress these perturbations and their associated variance. However, this does not directly address how these perturbations affect the mean flow itself. Just as we found the steady state variance of the perturbations, we will now solve for the steady-state eddy momentum flux divergence associated with the perturbations, and then use these eddy flux divergences to compute the tendency produced by these fluxes in the mean flow.

5.1 Evaluation of mean eddy momentum fluxes in a stochastically forced vortex

We would like to determine the mean eddy momentum flux divergence as a function of radius that is generated by a perturbation field driven stochastically as in (2.1). Recall that the eddy momentum flux divergence (which is equal to the local acceleration of the mean flow) at radius r is:

$$\frac{\partial}{\partial t}V(r,t) = -\frac{1}{r^2}\frac{\partial}{\partial r}(\overline{r^2 u'v'}) = -\overline{u'(r,t)\zeta'(r,t)} = -\frac{1}{4}[u^*(r,t)\zeta(r,t) + \zeta^*(r,t)u(r,t)] \quad (5.1)$$

The results over the whole domain for the averaged eddy fluxes can then be written in terms of the diagonal elements of a correlation matrix:

$$\mathbf{Y}^t_{ij} = -\frac{1}{4}(\langle u_i(t)\zeta_j{}^*(t)\rangle + \langle \zeta_i(t)u_j{}^*(t)\rangle) \quad (5.2)$$

where u and ζ now refer to the full vector representations of the radially varying perturbation velocity and vorticity functions for each azimuthal wavenumber.

We desire a way to find the steady-state eddy fluxes. We define a correlation matrix for vorticity $\mathbf{Z}^t$ such that:

$$\mathbf{Z}^t_{ij} = \langle \zeta_i(t)\zeta_j(t)\rangle \tag{5.3}$$

By comparison to (2.5) it is easy to see that we can solve for the steady state vorticity correlation matrix $\mathbf{Z}^\infty$ by exactly the same procedure we used to find $\mathbf{C}^\infty$; the result will depend on the time evolution operator $\mathbf{T}$ in vorticity coordinates rather than the operator $\mathbf{A}$ in generalized velocity coordinates. Farrell and Ioannou (1995) showed that any second-order moment of an arbitrary correlation matrix derived from arbitrary operators $\mathbf{L}_1$, $\mathbf{L}_2$:

$$\mathbf{S}_{ij} = \langle (\mathbf{L}_1 x)_i (\mathbf{L}_2 x)_j^* \rangle \tag{5.4}$$

can be found in terms of the operators and the correlation matrix (2.9) itself:

$$\mathbf{S} = \mathbf{L}_1 \mathbf{C} \mathbf{L}_2^\dagger \tag{5.5}$$

Recalling that the perturbation radial velocities can be found by operating on the vorticity with an operator based on the Green's function, we can use this result to find the steady state solution for the eddy flux divergence matrix $\mathbf{Y}^t$:

$$\mathbf{Y}^\infty = -\frac{1}{4}(\mathbf{U}\mathbf{Z}^\infty + \mathbf{Z}^\infty \mathbf{U}^\dagger) \tag{5.6}$$

where $\mathbf{U} = -ik\mathbf{R}^{-1}\mathbf{G}_k$ is the operator that obtains the radial perturbation velocities from the vorticity. Since the eddy flux divergence at each radius only depends on the local values of the velocity and vorticity [from (5.1)], the ensemble-averaged eddy flux divergence as a function of radius lies on the diagonal of the correlation matrix $\mathbf{Y}^\infty$.

5.2 Eddy flux divergence in the one-celled vortex

The mean eddy flux divergence for stochastically maintained perturbations in the one-celled vortex is shown in Figure 13 for azimuthal wavenumbers k=1, 2, and 16. For the lower wavenumbers we see that the net effect of the perturbations is to decelerate the flow in the vicinity

of the radius of maximum winds r=1, i.e., there is a downgradient momentum flux on average. For all wavenumbers $k > 8$ the net effect is to accelerate the flow in the vicinity of the radius of maximum winds, as shown in this case for k=16, so that there is on average an upgradient flux of momentum for azimuthal wavenumbers $k > 8$.

The reasons for this difference between the low- and high-wavenumber cases has previously been discussed to some extent by Nolan and Farrell (1998a) in the examination of the total eddy flux divergence over the lifetime of individual perturbations. It was found that whether or not the net momentum flux of a particular disturbance was upgradient or downgradient depended on the existence of nearly-neutral modes at that wavenumber (i.e., how close to zero was the real part of the eigenvalue of the least damped mode) and the extent to which these perturbations excited such modes. If they did, their energy would be trapped in the mode so that energy acquired from the mean flow through transient growth would not be effectively returned to the mean flow, resulting in a net downgradient momentum flux. If the energy is not trapped in this manner then most of the energy of the perturbation will eventually be returned to the mean flow, resulting in a net upgradient momentum flux. Our results here are therefore a generalization of those previous results to the case where all perturbations are excited equally.

5.3 Eddy flux divergence in the two-celled vortex

The mean eddy-flux divergence under stochastic forcing in the two-celled vortex is shown in Figure 14 for wavenumbers k=1, k=4, and k=8. The results for all three wavenumbers in this case are similar to the low-wavenumber results above in that the flow is being decelerated in the vicinity of the radius of maximum winds at r=2.19. However, the flow is being accelerated *inside* the radius of maximum winds, so that the mean momentum flux is inward rather than outward (but still downgradient). This result is similar to what was found by Lewellen et. al. (1997) in their

three-dimensional numerical simulations of a tornado vortex: the effect of the multiple vortices on the larger-scale flow was to transport angular momentum *inward.* The result for k=8 is different from the lower wavenumbers shown in several ways: first, the local accelerations are orders of magnitude smaller; second, the location of the maximum flow deceleration is at a slightly smaller radius, at r=2.0; thus the deceleration at r_{max}=2.19 is even smaller still; and third, there is a sus-btantial positive acceleration just outside the large negative acceleration in the vicinity of r_{max}. Thus for higher wavenumbers there are eddy momentum fluxes both outward and inward from the radius of maximum winds.

5.4 Resultant mean flow deviations

The two preceeding sections have shown us the ensemble-average acceleration to the mean vortex flow caused by a stochastically maintained perturbation field. However, this does not directly tell us what we really want to know, which is the change in the mean vortex flow resulting from these accelerations. This is because the mean vortex flow is experiencing the same advection due to the radial inflow and dissipation as the perturbations, as described by (3.3). Positive or negative perturbations to the symmetric azimuthal velocity function will be both advected into the core and smoothed by diffusion. Let us write the total perturbed symmetric flow as:

$$V(r,t) = \overline{V} + V'(r,t) \tag{5.7}$$

where $\overline{V}$ is the steady-state soultion to (3.3), and V' is its deviation. Substituting (5.7) into (3.3), and including the effects of the eddy flux divergences of the stochastically maintained perturbations, we have an equation for the evolution of the symmetric perturbations:

$$\frac{\partial}{\partial t}V' + U\frac{\partial}{\partial r}V' + \frac{UV'}{r} = \nu\left(\frac{\partial^2}{\partial r^2}V' + \frac{1}{r}\frac{\partial}{\partial r}V' - \frac{V'}{r^2}\right) - \sum_{k=1}^{n}\overline{u_k\zeta_k} \tag{5.8}$$

where the summation is over all the wavenumbers under consideration. In this report we will only

consider one wavenumber at a time. Once the ensemble average eddy flux divergence has been found from (5.6), we may solve for the ensemble-average solution for the mean flow deviation in a manner similar to the solution of (3.3) [see Nolan and Farrell (1998a)] by setting the time rate of change of V' to zero.

Figure 15 shows the ensemble-average mean flow deviation caused by stochastically maintained perturbations for k=1 and k=2 in the one-celled vortex. For k=1, we see that the mean flow is increased for r>1 and decreased for r<1. This is somewhat suprising, since the local effect of the perturbations is to decelerate the flow at r=1, as shown in Figure 13a. However, a closer examination of Figure 13a shows a small positive acceleration of the mean flow much farther outside the core of the vortex, in the vicinity of r=6. This positive anomaly is advected into the vortex core and amplified by conservation of angular momentum. Thus the effect of this small positive acceleration at large radius is to cause a substantial positive mean flow deviation at r=2 and to almost completely eliminate the effects of the large negative acceleration in the vortex core.

For k=2, the effect of positive accelerations at larger radius (see Figure 13b) is even more pronounced, such that the average mean flow deviation is positive everywhere, with a maximum near r=1.2, i.e., very close to the radius of maximum winds. Results for all higher wavenumbers were similar. Thus it appears that the presence of radial inflow has a substantial impact on how stochatically maintained perturbations ultimately effect the mean flow. To emphasize this point, we have recalculated the mean eddy flux divergences and the resultant average mean flow deviations in an identical one-celled vortex with the radial inflow eliminated. The results, shown in Figure 16, are strikingly different from before. Firstly, the predicted accelerations and mean flow changes are orders of magnitude larger than when the inflow was included. Secondly, we see that the ultimate effect of the perturbations for both k=1 and k=2 is to decrease the maximum windp-

seed and to increase the radius of maximum winds, i.e., to make the vortex broader and less intense.

The average mean flow deviations for k=1 and k=8 in the two-celled vortex are shown in Figure 17 (where the effects of radial inflow have again been included). We see that for k=1, the mean flow deviation is negative near the radius of maximum winds at r=2.19 and positive inside the vortex core. This result is very similar to what one might expect from examination of the average eddy flux divergence previously shown in Figure 14a. For k=8, however, we see that the average change in the mean flow is positive for all r! This again indicates the important effect of the radial inflow: small positive impulses outside the vortex core are carried inwards and intensified, so that the net effect on the mean flow is to increase the maximum windspeed.

The eddy momentum fluxes and resulting average mean flow deviations in the two-celled vortex recalculated without radial inflow are shown in Figure 18. The results here are analogous to what we saw for the one-celled vortex without radial inflow: for the lower, nearly unstable wavemumber k=1, the eddy flux divergences and mean flow deviations are orders of magnitude larger; for k=8, the formerly positive everywhere mean flow deviations are now negative in the vicinity of r_{max}.

6 Discussion

6.1 The least damped mode as a determining factor in the stochastic dynamics

While a variety of linear perturbation dynamics have been observed in the preceeding sections, the results of stochastic forcing of our two vortex types can generally be separated into two cases:

Case I: the stochastic forcing excites transient growth of initially upshear-tilted perturbations which are sheared over by the mean flow, reach their maximum energy when they have

evolved into a large-scale structure, then are sheared over further and give their energy back to the mean flow. While a small amount of energy is lost to dissipation along the way, almost all the initial disturbance energy and the energy acquired from the mean flow during the growth phase are returned to the mean flow through upgradient eddy momentum fluxes. In this case the input energy of the stochastic forcings ends up in the mean flow and the vortex is intensified.

Case II: again, the stochastic forcing excites transient growth; however, in this case the decay rate of the least damped mode is extremely small (for example, the least damped mode decay rate is 2.1×10^{-3} for k=1 in the one-celled vortex and 9.3×10^{-4} for k=3 in the the two-celled vortex) and these modes are also similar in structure to the coherent structures that the transiently growing disturbances become when they reach their maximum energy. The transiently growing disturbances then project strongly onto the least damped modes and their energy is trapped there; in other words, the least damped modes interact with the mean flow vorticity gradient so that they sustain themselves and are not sheared over by the mean flow. In this case, disturbance energy "accumulates" in the nearly-neutral modes and the energy is not returned to the mean flow, but is instead lost through dissipation very slowly over long times. Since the disturbances are never sheared over to cause upgradient momentum fluxes, only downgradient momentum fluxes occur and the vortex is weakened.

In this latter case, the sustained variance can be orders of magnitude larger than in Case I. From examining these two cases we gain more insight into why the presence of radial inflow has such a substantial effect on the results: including the effects of radial inflow has the stablizing effect of increasing the decay rates of the least damped modes for the cases of k=1 in the one-celled vortex and k=1, k=2, and k=3 for the two-celled vortex.

Similar observations and analysis have been reported for stochastic forcing of linearized

disturbances for examples such as unbounded constant shear flows (Farrell and Ioannou, 1993a), plane Couette and Poiseuille flows (Farrell and Ioannou, 1993b), and for barotropic and baroclinic dynamics in mid-latitude jets (Farrell and Ioannou, 1995; DelSole and Farrell, 1996).

6.2 Discussion in context with recent results regarding tropical cyclones

As mentioned in the introduction, asymmetric disturbances have received considerable attention in connection with tropical cyclone dynamics, with much of the emphasis on how these disturbances affect the tropical cyclone track and on their relationship to spiral bands. However, asymmetric dynamics have also been considered as a mechanism for hurricane intensification, originally by Pfeffer (1958) and more recently by Challa and Pfeffer (1980), Pfeffer and Challa (1981), Carr and Williams (1989), Montgomery and Kallenbach (1997) and Montgomery and Enaganio (1997). In this last report the authors used a three-dimensional quasigeostrophic model to demonstrate how coherent potential vorticity anomalies, injected in bursts so as to model episodic convection, are sheared over by the larger-scale vortex flow and ultimately cause upgradient momentum fluxes.

While the works cited above have focused specifically on tropical cyclones, the previous reports by Nolan (1996), Nolan and Farrell (1998a) and this report have attempted to generalize the phenomena of asymmetric vortex intensification to a wider class of vortices sustained by convergence and also to a wider class of asymmetric forcings. One major distinction between our work and most of the works cited in the introduction and above [except Carr and Williams (1989)] is that both our mean vortex flows transition to a potential ($1/r$) vortex outside of the radius of maximum winds. A potential flow has no vorticity, so there is no mechanism for the propagation of waves away from the vortex. The azimuthal wind fields of huricanes generally have a slower decay with radius, such as $1/r^{1/2}$, which allows for the existence of waves on the associated mean

vorticity gradient. Such waves, sometimes called "vortex-Rossby waves" were examined by Montgomery and Kallenbach (1997), who explained their dynamics and showed how downshear tilted disturbances alway propagate away from the core of the vortex. In our case, however, there are no such waves in the potential flow region and the phenomenon of wave momentum and energy transport away from the vortex does not occur. However, M.T. Montgomery has pointed out (1997, personal communcation) that there may be vortex-Rossby waves occuring within the parts of the mean flow that do have mean vorticity, and that these waves may influence the complex structures of the eddy flux divergence fields as shown in Figure 13 and Figure 14. This remains for further study.

7 Conclusions

In this report we have extended the earlier analysis of Nolan and Farrell (1998a) to examine the response of a vortex with radial inflow to random forcing by asymmetric disturbances. The results have shown that under stochastic forcing that is unbiased in space and time, the previously identified global optimals play a dominat role in the transfer of energy from the mean flow to the perturbations. For stable wavenumbers where nearly-neutral (i.e., almost unstable) modes are present, the variance excited by the stochastic forcing and amplified by wave-mean flow interactions can be very large. This variance is greatly overestimated if the effects of the radial inflow that sustains the mean flow are neglected in the dynamics of the perturbations.

For all but the lowest, stable wavenumbers in both one- and two-celled vortices the net effect of the eddy momentum fluxes associated with the stochastically maintained perturbations is to intensify the vortex, i.e., to increase the maximum windspeed. We also note the important observation that this effect is enhanced by the presence of the radial inflow, and that neglecting the dynamical effects of the radial inflow in these vortices produces quite opposite results in some

cases. Thus we have shown that even when there is continuous excitation of perturbations that are favorably configured for transient growth (and therefore cause downgradient momentum flux), the radial inflow which sustains the mean vortex will help to ensure that the net effect of these disturbances will be to cause (on average) upgradient eddy momentum fluxes and to intensify the vortex.

The two-dimensional vortex flows with radial inflow that we have constructed are certianly crude models of intense atmopsheric vortices, and our analysis neglects all three-dimensional dynamics which may be important. We have, however, shown how disturbances which are either generated within the vortex itself (such as mesoscale bursts of convection in tropical cyclones), or are carried into the vortex core by the convergent radial inflow (such as boundary-layer turbulence in the surrounding environment of a tornado), can contribute to the intensification and maintenance of these vortices by causing upgradient momentum fluxes and transferring their kinetic energy to the mean flow. In the future, we plan to extend this type of analysis to three-dimensional perturbations in more realistic, three-dimensional or axisymmetric representations of intense atmospheric vortices.

Acknowledgements

The authors would like to thank M. Montgomery for many helpful comments and advice on hurricane dynamics, and P. Ioannou and T. DelSole for many helpful discussions. We would also especially like to thank D. Adalsteinsson for helping us to make tremendous improvements in the production and appearance of our contour plots. Preliminary work for this report was prepared as part of the Ph.D. thesis of D. Nolan while he was a student at Harvard University, during which he was supported by NSF Grant ATM-9216813 and NSF Grant 9623539; since November of 1996 D. Nolan has been supported by the Applied Mathematical Sciences Subprogram of the Office of Energy Research, U.S. Department of Energy under contract DE-AC03-76SF-00098. B. Farrell was supported by NSF Grant ATM-9216813 and NSF Grant 9623539.

References

Burgers, J. M., 1948: A mathematical model illustrating the theory of turbulence. *Adv. Appl. Mech.*, **1**, pp. 197-199.

Carr, L. E. III, and R. T. Williams, 1989: Barotropic vortex stability to perturbations from axisymmetry. *J. Atmos. Sci.*, **46**, pp. 3177-3191.

Case, K. M., 1960: Stability of plane Couette flow. *Phys. Fluids*, **8**, pp. 143-148.

Challa, M., and R. L. Pfeffer, 1980: Effects of eddy fluxes of angular momentum on model hurricane development. *J. Atmos. Sci.*, **37**, pp. 1603-1618.

DelSole, Timothy M., 1993: Absolutley Unstable and Stochastically Forced Baroclinic Waves. Ph.D. Thesis, Harvard University, 216 pp.

----------, and Brian F. Farrell, 1996: The quasilinear equilibration of a thermally maintained, stochastically excited jet in a two-layer model. *J. Atmos. Sci.*, **53**, pp. 1781-1797.

Emanuel, Kerry, 1984: A note on the stability of columnar vortices. *J. Fluid Mech.*, **145**, pp. 235-238.

Farrell, Brian F., 1988: Optimal excitation of neutral Rossby waves. *J. Atmos Sci.*, **45**, pp. 163-172.

----------, 1989: Transient development in confluent and difluent flow. *J. Atmos. Sci.*, **46**, pp. 3279-3288.

Farrell, Brian F., and Petros J. Ioannou, 1993: Stochastic forcing of the linearized Navier-Stokes equations. *Phys. Fluids A*, **5**, pp. 2600-2609.

----------, and ----------, 1994: A theory for the statistical equilibrium energy spectrum and heat flux produced by transient baroclinic waves. *J. Atmos. Sci.*, **51**, pp. 2658-2698.

----------, and ----------, 1996: Generalized stability theory. Part I: Autonomous operators. *J. Atmos. Sci.*, **53**, pp. 2025-2040.

Fiedler, Brian H., 1998: Windspeed limits in numerically-simulated tornadoes with suction vortices. *Q. J. R. Meteorol.Soc.*, to appear.

Flierl, Glenn R., 1988: On the instability of geostrophic vortices. *J. Fluid Mech.*, **197**, pp. 349-388.

Fujita, T. T., 1971: Proposed mechanism of suction spots accompanied by tornadoes. In *Preprints, 7th Conference on Severe Local Storms*, pp. 208-213, American Meteorological Society, Boston, Mass.

Gall, R. L., 1983: A linear analysis of the multiple vortex phenomenon in simulated tornadoes. *J. Atmos. Sci.*, **40**, pp. 2010-2024.

----------, 1985: Linear dynamics of the multiple-vortex phenomenon in tornadoes. *J. Atmos. Sci.*, **42**, pp. 761-772.

Gardiner, C. W., 1985: *Handbook of Stochastic Methods*. 2d ed. Springer-Verlag, 442 pp.

Guinn, Thomas A., and Wayne H. Schubert, 1993: Hurricane sprial bands. *J. Atmos. Sci.*, **50**, pp. 3380-3403.

Kallenbach, R. J., and M. T. Montgomery, 1995: Symmetrization and hurricane motion in an asymmetric balance model. *21st Conference on Hurricanes and Tropical Meteorology.* Americal Meteorological Society, pp. 103-105.

Kurihara, Y., 1976: On the development of spiral bands in a tropical cyclone. *J. Atmos. Sci.*, **33**, 940-958.

Leibovich, S., and K. Stewartson, 1983: A sufficient condition for the instability of columnar vortices. *J. Fluid Mech.*, **126**, pp. 335-356.

Lewellen, W. S., D. C. Lewellen, and R. I. Sykes, 1997: Large-eddy simulation of a tornado's interaction with the surface. *J. Atmos. Sci.*, **54**, pp. 581-605.

Montgomery, Michael T., and Randall J. Kallenbach, 1997: A theory for vortex Rossby waves and its application to spiral bands and intensity changes in hurricanes. *Q. J. Roy. Meteorol. Soc.*, **123**, pp. 435-465.

----------, and Janice Enaganio, 1997: Tropical cyclogenesis via convectively forced vortex Rossby waves in a three-dimensional quasigeostrophic model. *J. Atmos. Sci.*, to appear.

Nolan, David S., 1996: Axisymmetric and Asymmetric Vortex Dynamics in Convergent Flows. Ph.D. Thesis, Harvard University. [Available from University Microfilm, 305 N. Zeeb Rd., Ann Arbor, MI 48106.]

----------, and Brian F. Farrell, 1998a: Generalized stability analyses of asymmetric disturbances in one- and two-celled vortices maintained by radial inflow. Accepted pending revision to *J. Atmos. Sci.*

----------, 1998b: On the structure and dynamics of tornado-like vortices. Submitted to *J. Atmos. Sci.*

Orr, W. Mc'F., 1907: Stability or instability of the steady motions of a perfect liquid. *Proc. Roy. Irish Acad.*, **27**, pp. 9-69.

Pfeffer, R. L., 1958: Concerning the mechanics of hurricanes. *J. Meteor.*, **15**, pp. 113-120.

----------, and M. Challa, 1981: A numerical study of the role of eddy fluxes of momentum in the development of Atlantic hurricanes. *J. Atmos. Sci.*, **38**, pp. 2393-2398.

Peng, Melinda S., and R. T. Williams, 1991: Stability analysis of barotropic vortices. *Geophys. and Astrophys. Fluid Dynamics*, **58**, pp. 263-283.

Rayleigh, Lord, 1880: On the stability and instability of certain fluid motions. *Proc. London Math. Soc.*, **11**, pp. 57-70.

Robinson, A. C., and P. G. Saffman, 1984: Stability and structure of stretched vortices. *Stud. Appl. Math.*, **70**, pp. 163-180.

Rott, N., 1958: On the viscous core of a line vortex. *Z. Agnew Math. Mech.*, **9**, pp. 543-553.

Rotunno, Richard, 1978: A note on the stability of a cylindrical vortex sheet. *J. Fluid Mech.*, **87**, pp. 761-771.

Shapiro, Lloyd J., 1992: Hurricane vortex motion in a three-layer model. *J. Atmos. Sci.*, **108**, pp. 401-421.

Shepherd, Theodore G., 1985: Time development of small disturbances to plane Couette flow. *J. Atmos. Sci.*, **42**, pp. 1868-1871.

Smith, Gerald B. II, and Michael T. Montgomery, 1995: Vortex axisymmetrization: Dependence on azimuthal wavenumber or asymmetric radial structure changes. *Q. J. Roy. Met. Soc.*, **121**, pp. 1615-1650.

Smith, R. K., and H. C. Weber, 1993: An extended analytic theory of tropical-cyclone motion in a a barotropic shear flow. *Q. J. R. Meteorol. Soc.*, **119**, pp. 1149-1166.

Staley, D. O., 1985: Effect of viscosity on inertial instability in a tornado vortex. *J. Atmos. Sci.*, **42**, pp. 293-297.

----------, and R. L. Gall, 1979: Barotropic instability in a tornado vortex. *J. Atmos. Sci.*, **36**, pp. 973-981.

----------, and ----------, 1984: Hydrodynamic instability of small eddies in a tornado vortex. *J. Atmos. Sci.*, **41**, pp. 422-429.

Steffens, Jerry L., 1988: The effect of vorticity-profile shape on the instability of a two-dimensional vortex. *J. Atmos. Sci.*, **45**, pp. 254-259.

Thompson, W., 1887: Stability of fluid motion: rectilinear motion of viscous fluid between two parallel planes. *Phil. Mag.*, **24**, 188-196.

Willoughby, H. E., 1992: Linear motion of a shallow-water barotropic vortex as an initial-value problem. *J. Atmos. Sci.*, **49**, pp. 2015-2031.

----------, 1994: Nonlinear motion of a shallow water barotropic vortex. *J. Atmos. Sci.*, **51**, pp. 3722-3744.

Figure Captions

Figure 1. Profiles of radial and and azimuthal velocity for the one-celled vortex: a) radial velocity; b) azimuthal velocity; c) negative horizontal divergence (stretching); d) vorticity gradient.

Figure 2. Profiles of radial and and azimuthal velocity for the two-celled vortex: a) radial velocity; b) azimuthal velocity; c) negative horizontal divergence (stretching); d) vorticity gradient.

Figure 3. The real part of the least damped mode as a function of azimuthal wavenumber (stability diagram) for the two-celled vortex; o's: with the radial inflow effects included in the perturbation dynamics; x's: with the radial inflow effects negelected.

Figure 4. Stochastic optimals (SOs) for k=1 and k=2 in the one-celled vortex: a) k=1 vorticity; b) k=1 streamfunction; c) k=2 vorticity; d) k=2 streamfunction. Their fractional contribution to the variance is listed at the top of each plot.

Figure 5. Empirical orthogonal functions (EOFs) for k=1 and k=2 in the one-celled vortex: a) k=1 vorticity; b) k=1 streamfunction; c) k=2 vorticity; d) k=2 streamfunction. Their fractional representation of the variance is listed at the top of each plot.

Figure 6. The global optimal and its structure at the moment of maximum energy (realized global optimal) for k=1 in the one-celled vortex: a) GO vorticity; b) GO streamfunction; c) RGO vorticity; d) RGO streamfunction.

Figure 7. Stochastic optimals (SOs) for k=1 and k=3 in the two-celled vortex: a) k=1 vorticity; b) k=1 streamfunction; c) k=3 vorticity; d) k=3 streamfunction. Their fractional contribution to the variance is listed at the top of each plot.

Figure 8. Empirical orthogonal functions (EOFs) for k=1 and k=3 in the two-celled vortex: a) k=1 vorticity; b) k=1 streamfunction; c) k=3 vorticity; d) k=3 streamfunction. Their fractional representation of the variance is listed at the top of each plot.

Figure 9. The global optimal and its structure at the moment of maximum energy (realized global optimal) for k=3 in the two-celled vortex: a) GO vorticity; b) GO streamfunction; c) RGO vorticity; d) RGO streamfunction.

Figure 10. The sustained variance in the a) the one-celled vortex and b) the two-celled vortex under stochastic forcing as a function of azimuthal wavenumber: o's - the standard variance; x's - the same variance with the radial inflow effects neglected; +'s - the equivalent normal variance of the vortices with inflow. The variance without inflow is not shown for k=2 and k=3 because the vortex is unstable without inflow for these wavenumbers.

Figure 11. Perturbation variance sustained under unitary stochastic forcing in the one-celled vortex as a function of the strength of the radial inflow, calculated with (o's) and without (x's) the dynamical terms associated with radial inflow, and also for an normal system with the same spectrum (+'s): a) for k=1; b) for k=2.

Figure 12. Perturbation variance sustained under unitary stochastic forcing in the two-celled vortex as a function of the strength of the radial inflow, calculated with (o's) and without (x's) the dynamical terms associated with radial inflow, and also for a normal system with the

same spectrum (+'s): a) for k=1; b) for k=8.

Figure 13. Mean eddy flux divergence caused by perturbations sustained by stochastic forcing in the one-celled vortex: a) for k=1; b) for k=2; c) for k=16.

Figure 14. The ensemble-average eddy flux divergences associated with the stochastically maintained perturbations in the two-celled vortex: a) for k=1; b) for k=4; c) for k=8.

Figure 15. The resulting average mean flow deviations caused by the stochastically maintained eddy flux divergence in the one-celled vortex: a) k=1; b) k=2.

Figure 16. The average eddy flux diverences and resultant mean flow deviations in the one-celled vortex, recomputed with the radial inflow eliminated: a) average eddy flux diveregnce, k=1; b) average mean flow deviation, k=1; c) average eddy flux divergence, k=2; d) average mean flow deviation, k=2.

Figure 17. The average mean flow deviations in the two-celled vortex caused by the stochastically maintained perturbations: a) for k=4; b) k=8.

Figure 18. The average eddy flux diverences and resultant mean flow deviations in the two-celled vortex, recomputed with the radial inflow eliminated: a) average eddy flux diveregnce, k=4; b) average mean flow deviation, k=4; c) average eddy flux divergence, k=8; d) average mean flow deviation, k=8.

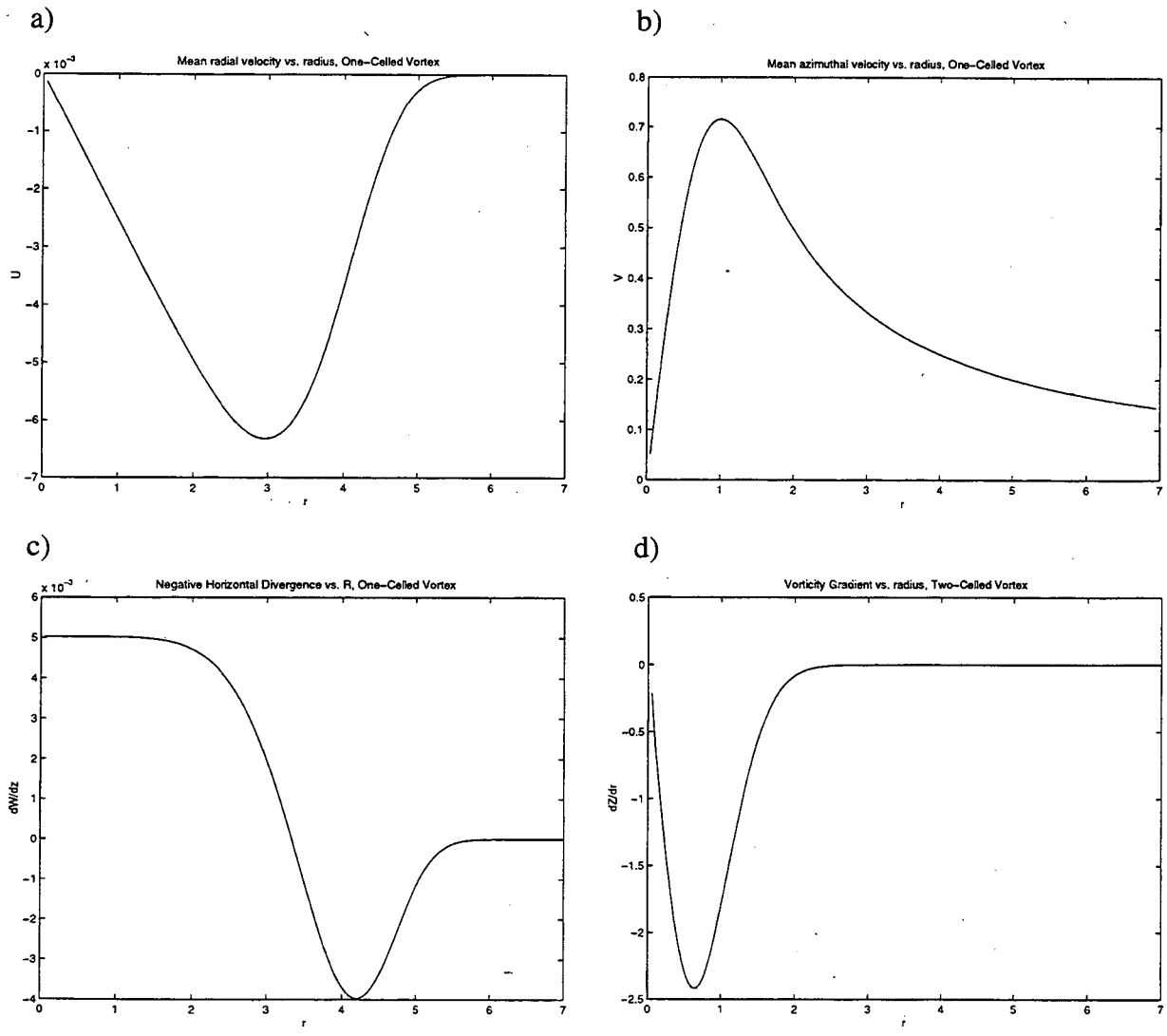

Figure 1 Profiles of radial and and azimuthal velocity for the one-celled vortex: a) radial velocity; b) azimuthal velocity; c) negative horizontal divergence (stretching); d) vorticity gradient.

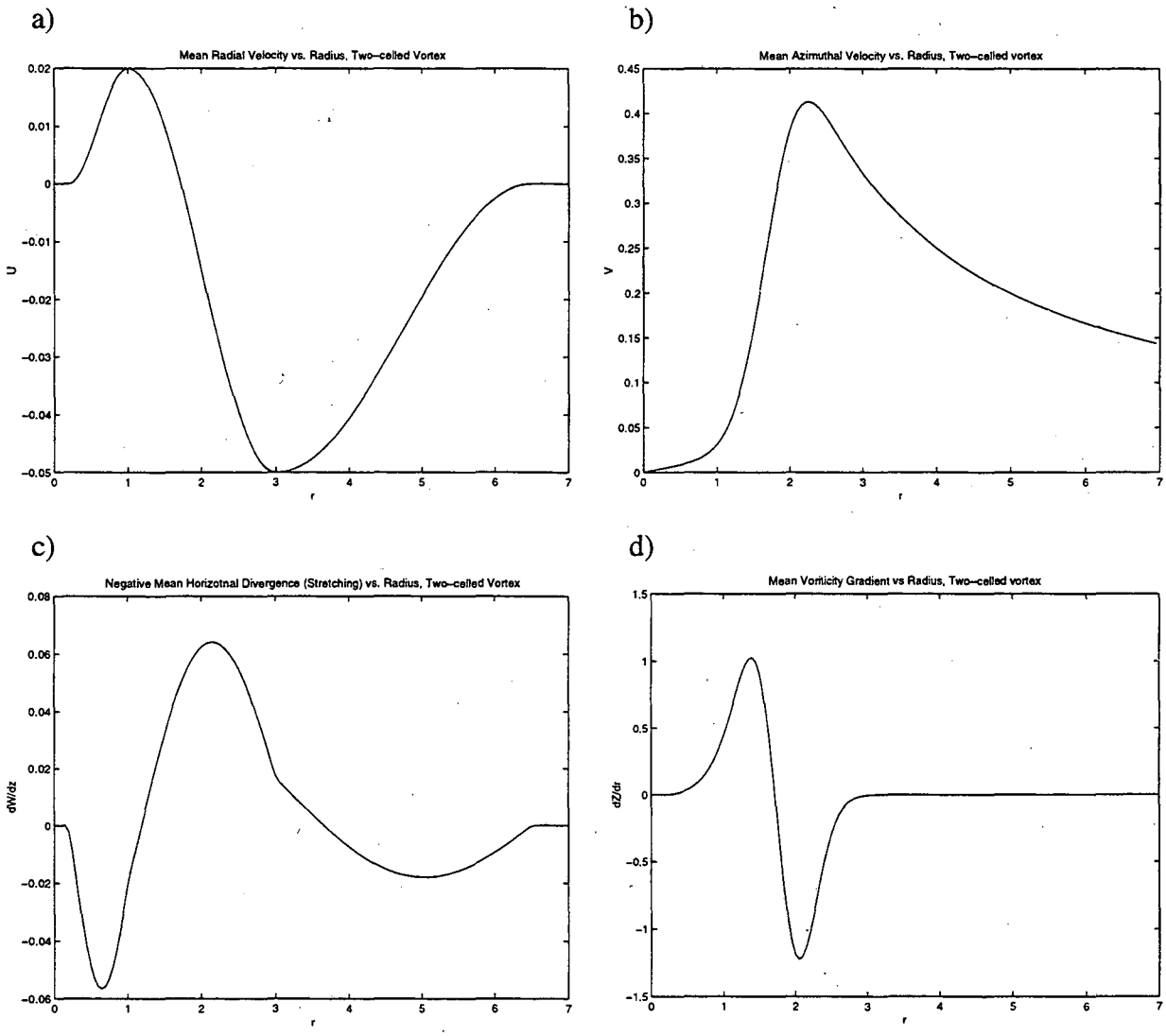

Figure 2 Profiles of radial and and azimuthal velocity for the two-celled vortex: a) radial velocity; b) azimuthal velocity; c) negative horizontal divergence (stretching); d) vorticity gradient.

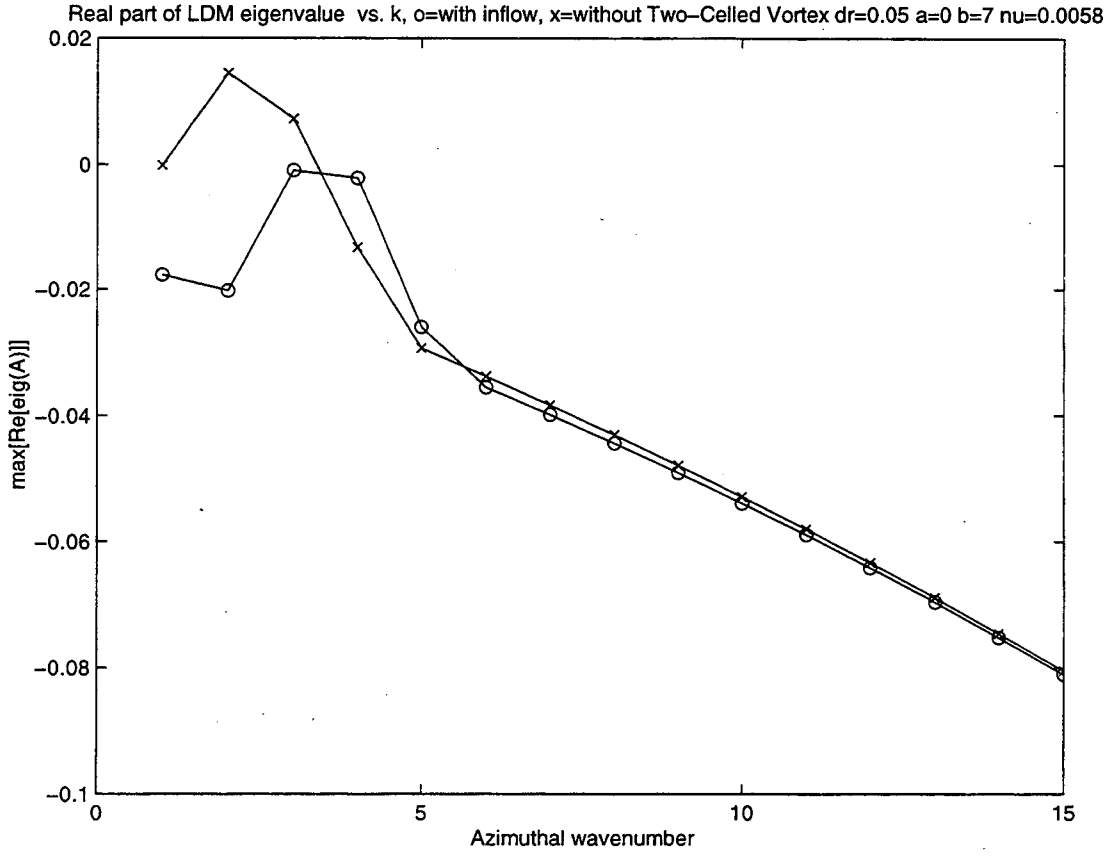

Figure 3 The real part of the least damped mode as a function of azimuthal wavenumber (stability diagram) for the two-celled vortex; o's: with the radial inflow effects included in the perturbation dynamics; x's: with the radial inflow effects negelected.

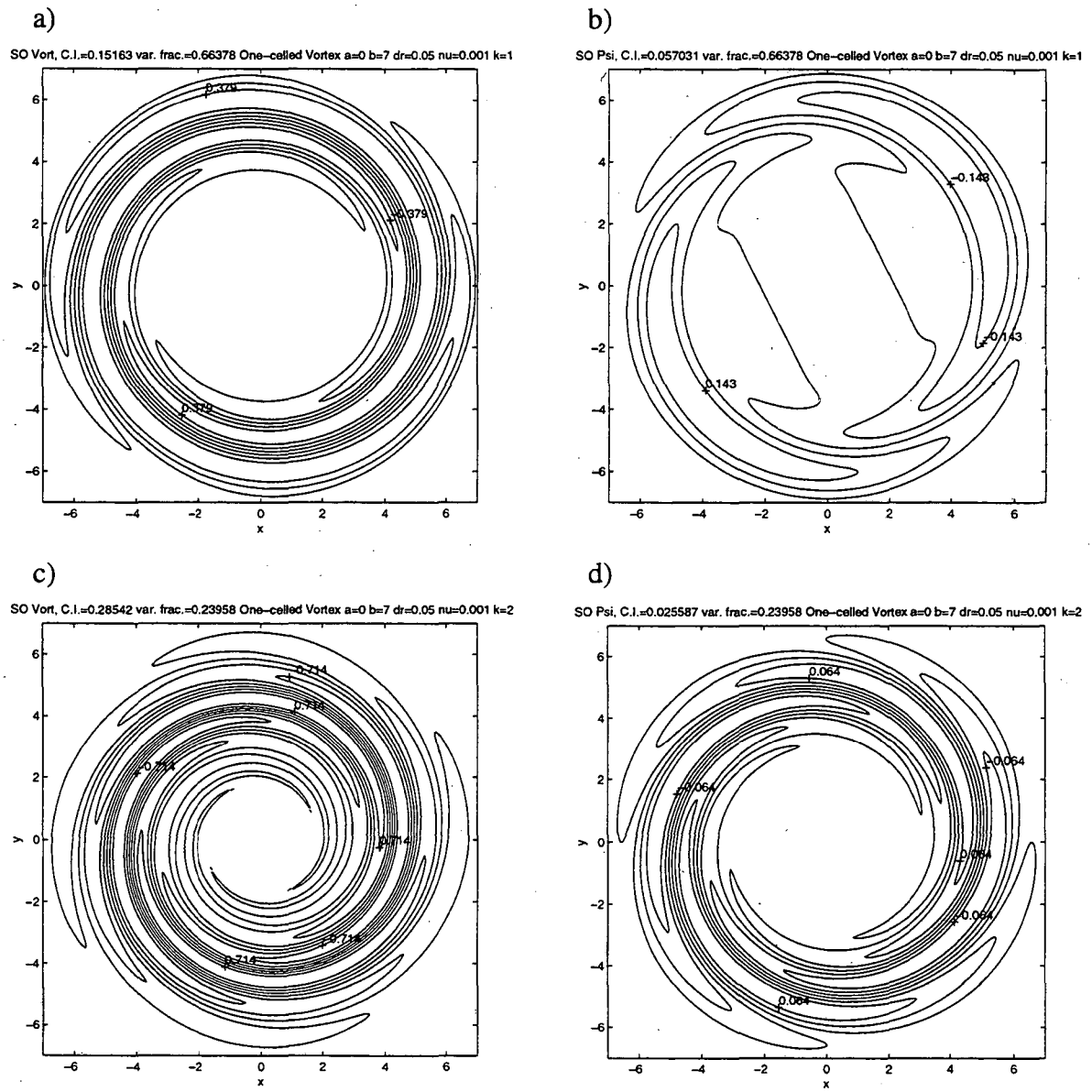

Figure 4 Stochastic optimals (SOs) for k=1 and k=2 in the one-celled vortex: a) k=1 vorticity; b) k=1 streamfunction; c) k=2 vorticity; d) k=2 streamfunction. Their fractional contribution to the variance is listed at the top of each plot.

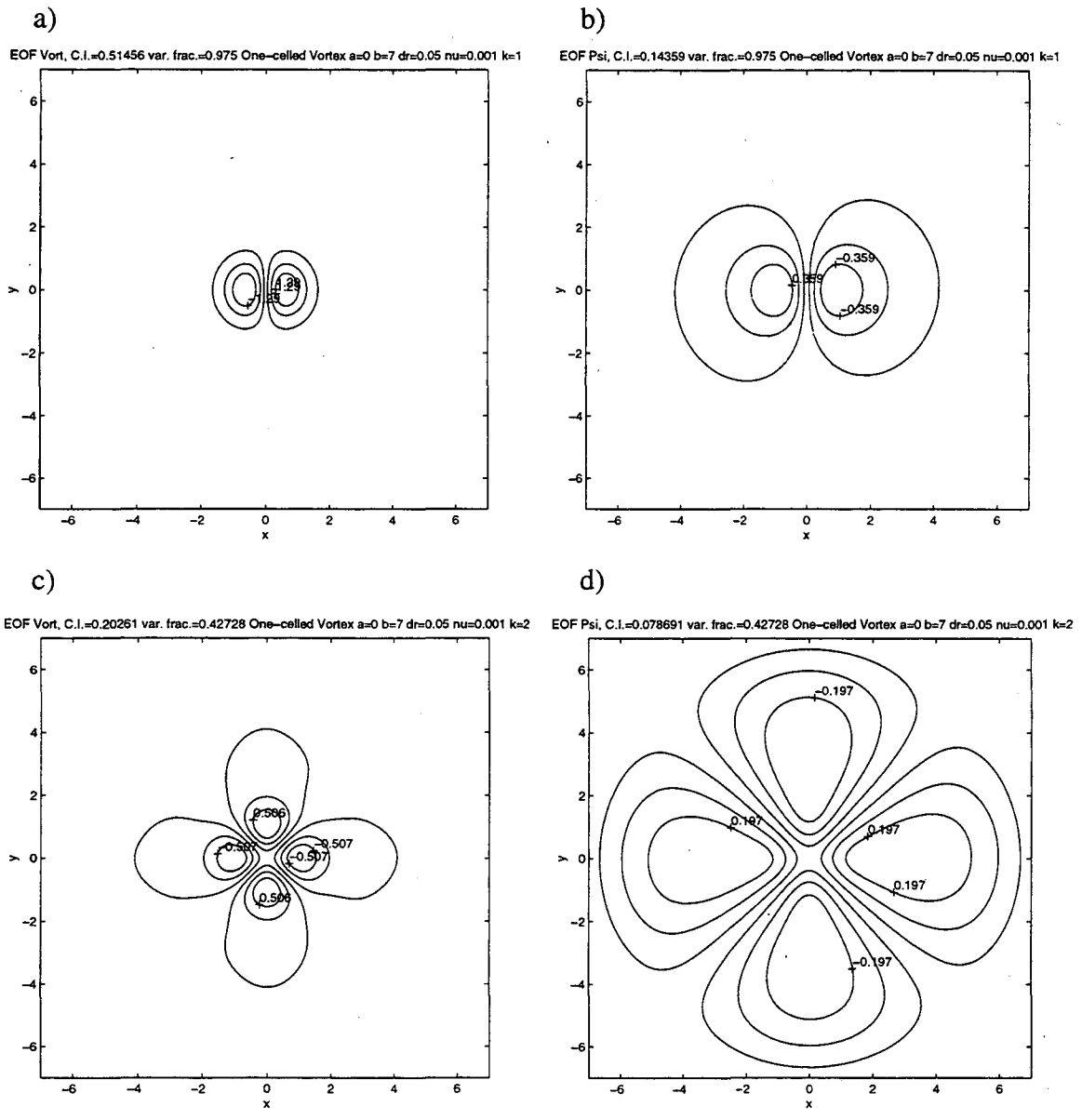

Figure 5 Empirical orthogonal functions (EOFs) for k=1 and k=2 in the one-celled vortex: a) k=1 vorticity; b) k=1 streamfunction; c) k=2 vorticity; d) k=2 streamfunction. Their fractional representation of the variance is listed at the top of each plot.

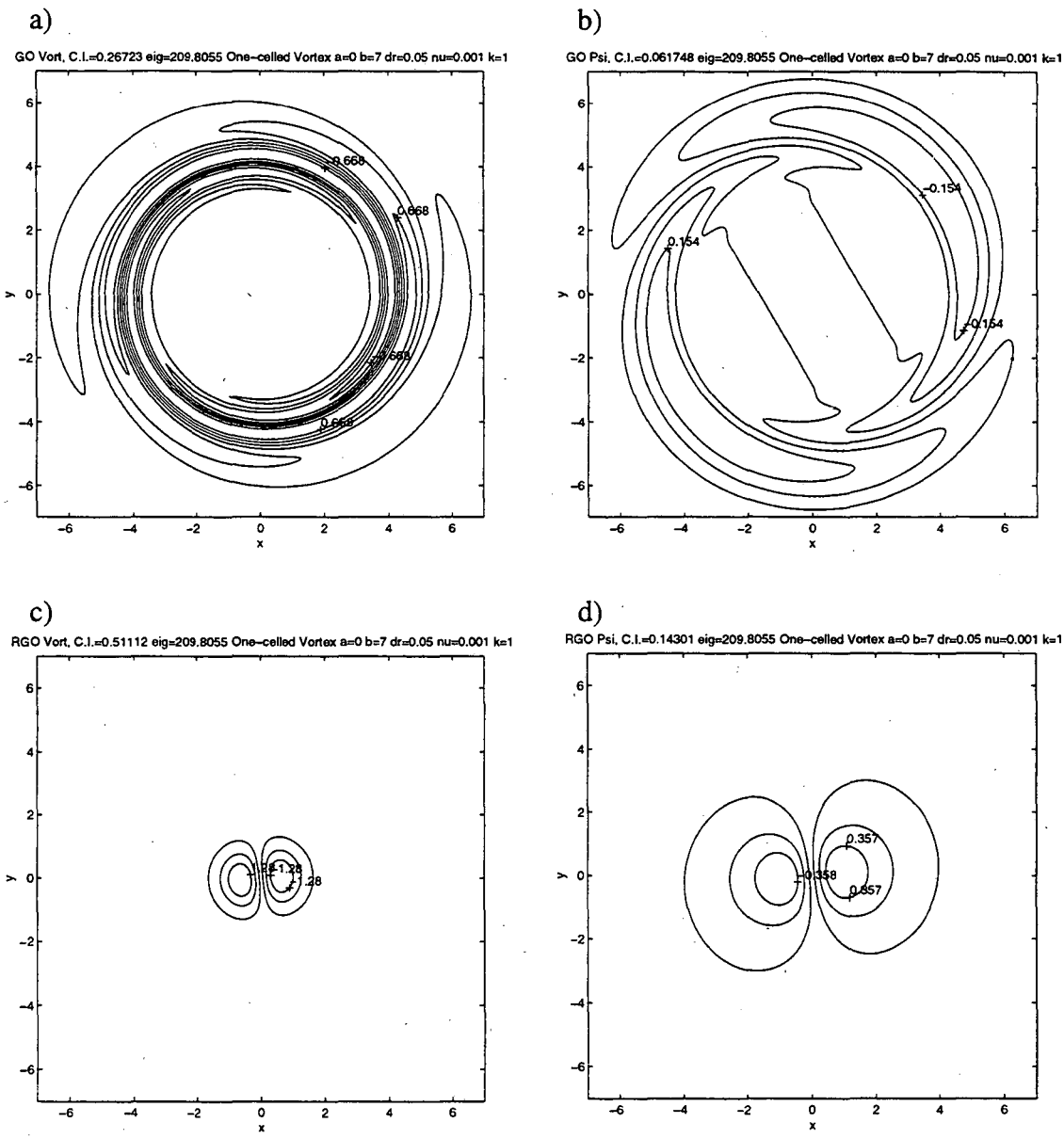

Figure 6 The global optimal and its structure at the moment of maximum energy (realized global optimal) for k=1 in the one-celled vortex: a) GO vorticity; b) GO streamfunction; c) RGO vorticity; d) RGO streamfunction.

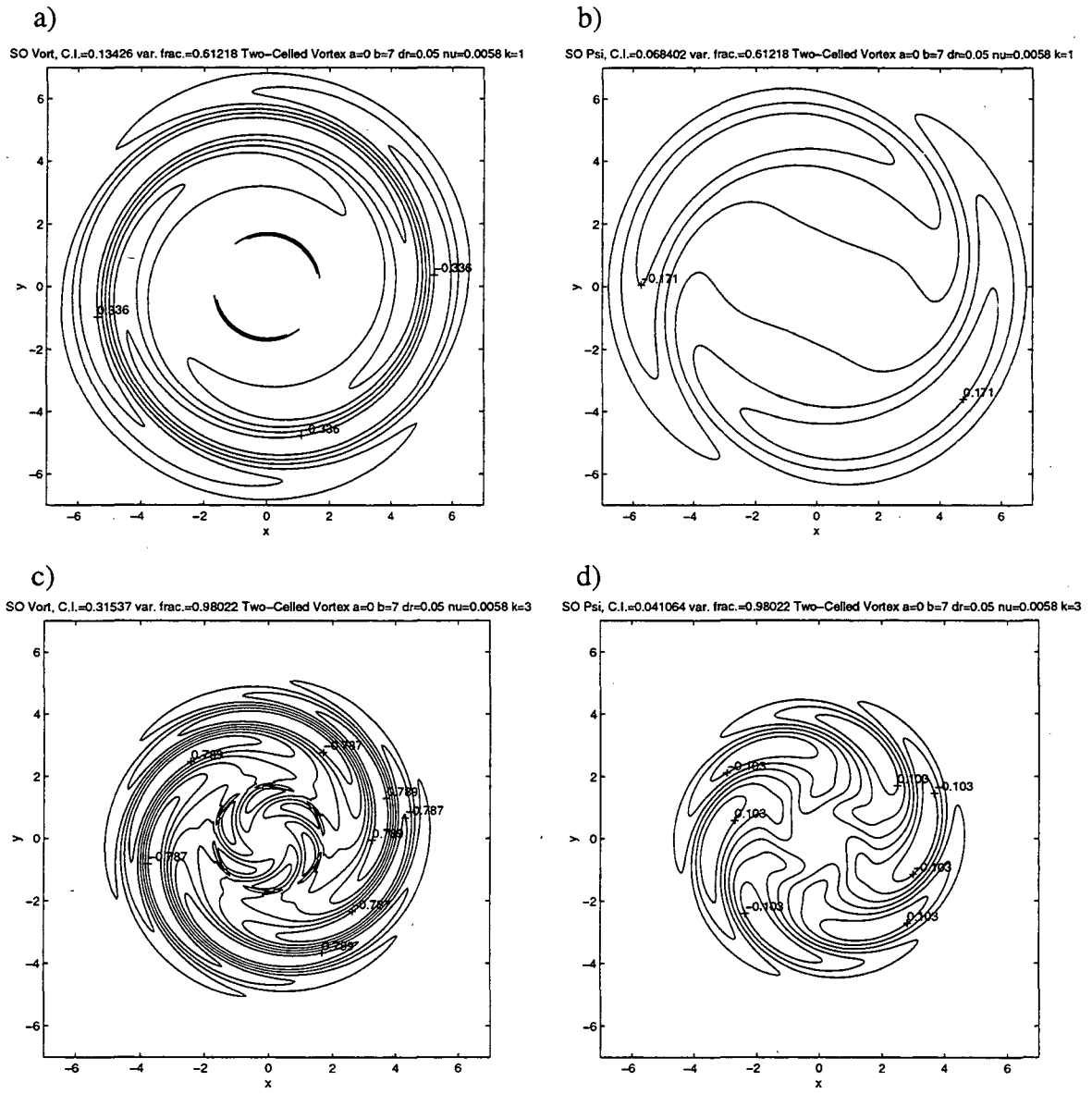

Figure 7 Stochastic optimals (SOs) for k=1 and k=3 in the two-celled vortex: a) k=1 vorticity; b) k=1 streamfunction; c) k=3 vorticity; d) k=3 streamfunction. Their fractional contribution to the variance is listed at the top of each plot.

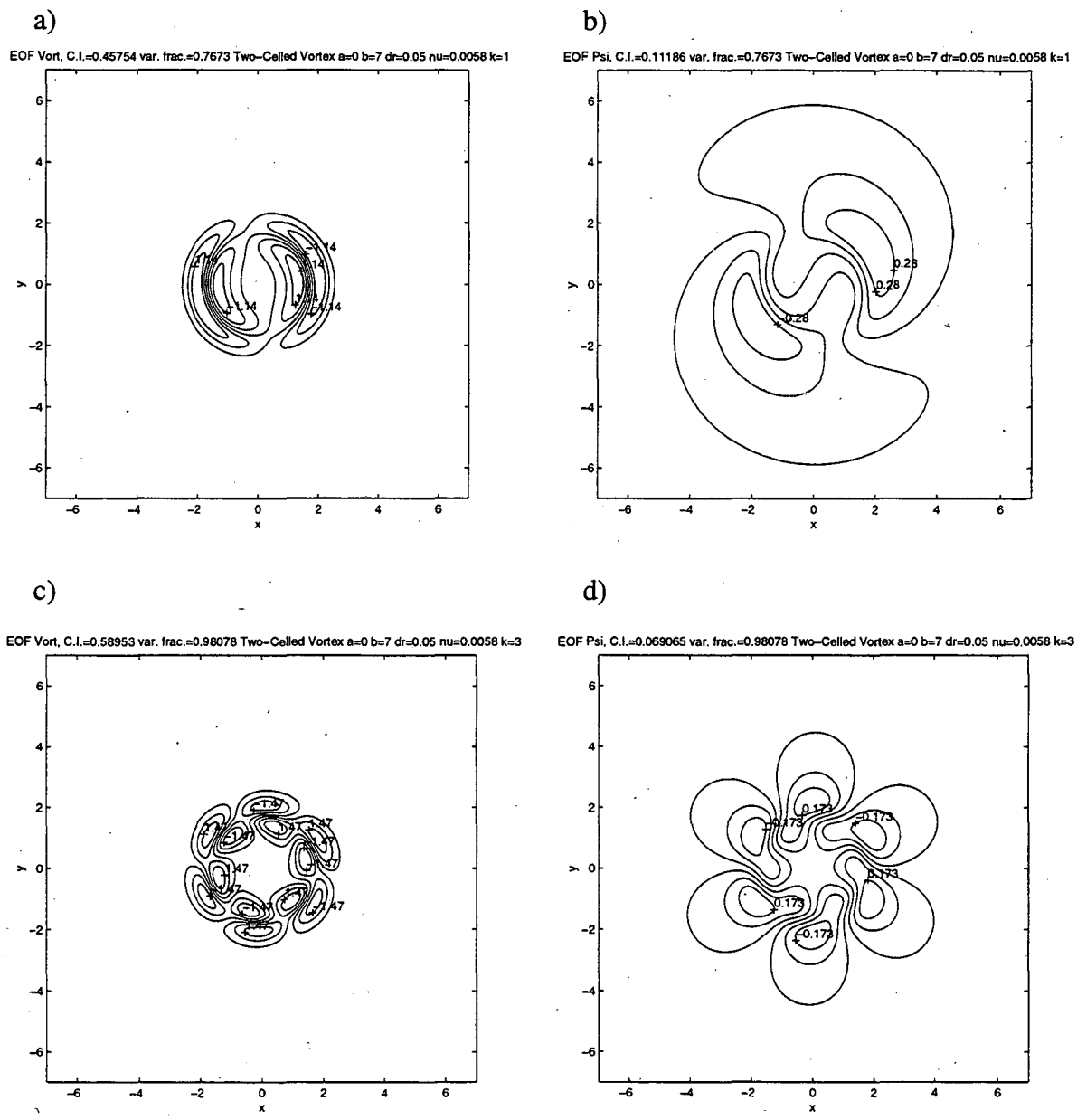

Figure 8 Empirical orthogonal functions (EOFs) for k=1 and k=3 in the two-celled vortex: a) k=1 vorticity; b) k=1 streamfunction; c) k=3 vorticity; d) k=3 streamfunction. Their fractional representation of the variance is listed at the top of each plot.

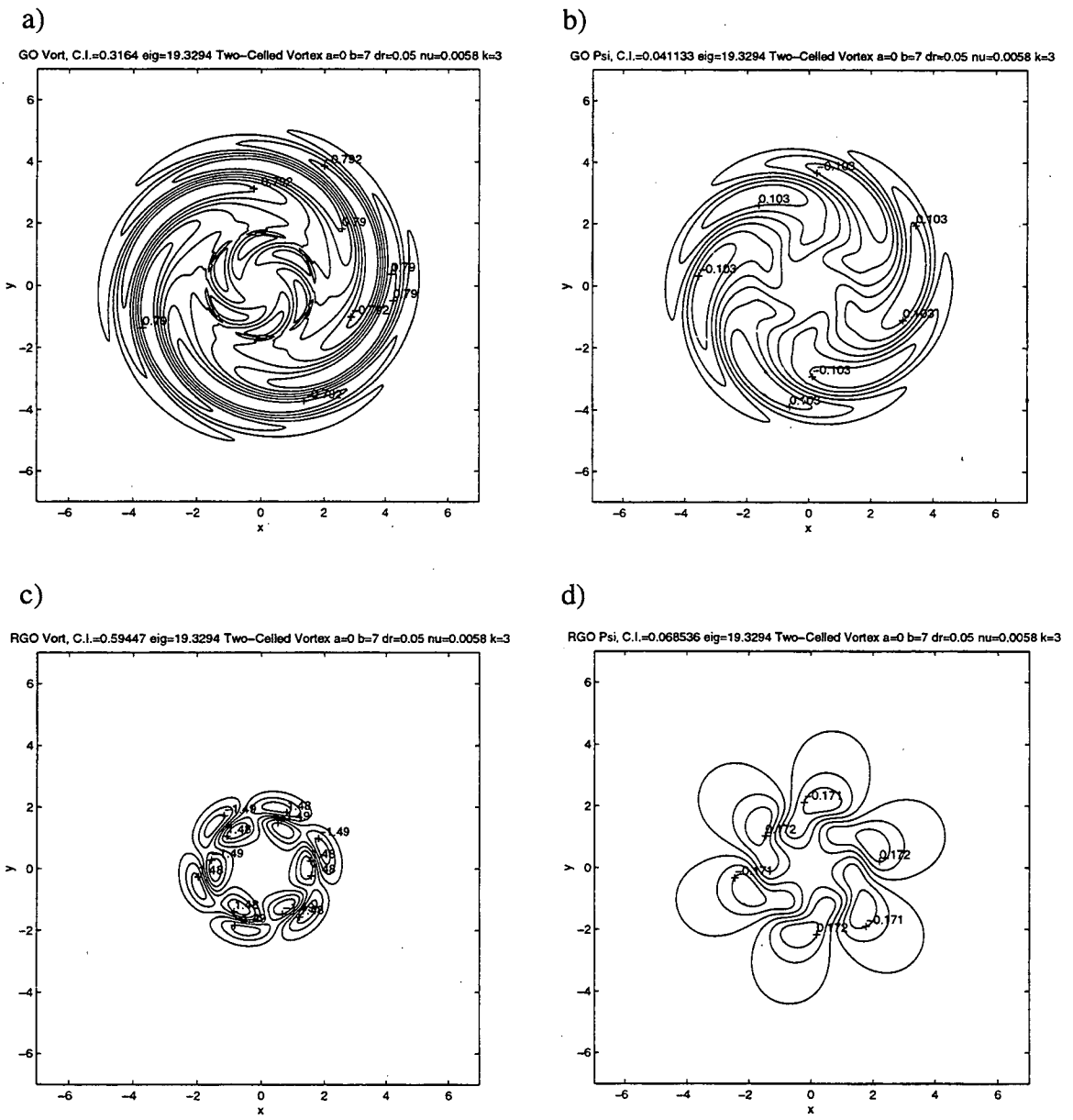

Figure 9 The global optimal and its structure at the moment of maximum energy (realized global optimal) for k=3 in the two-celled vortex: a) GO vorticity; b) GO streamfunction; c) RGO vorticity; d) RGO streamfunction.

a)

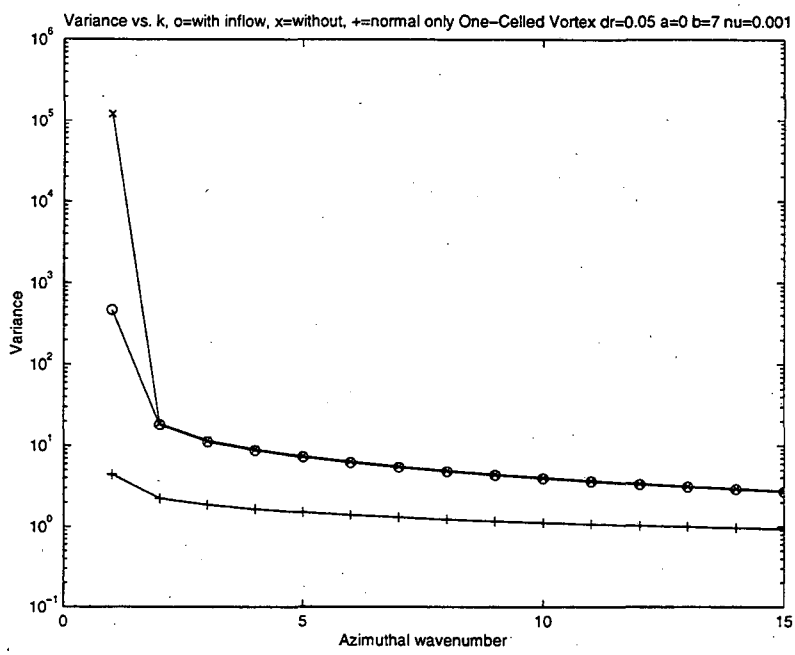

b)

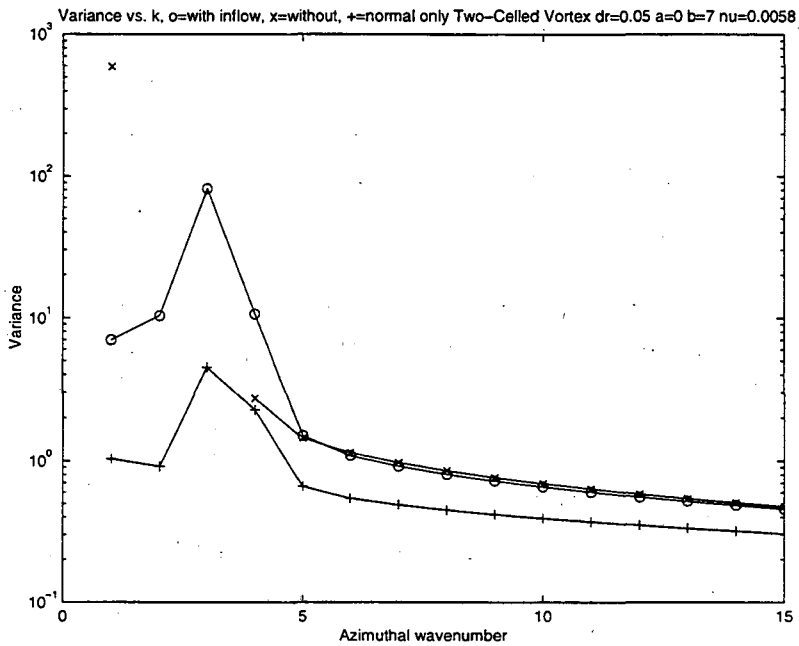

Figure 10 The sustained variance in the a) the one-celled vortex and b) the two-celled vortex under stochastic forcing as a function of azimuthal wavenumber: o's - the standard variance; x's - the same variance with the radial inflow effects neglected; +'s - the equivalent normal variance of the vortices with inflow. The variance without inflow is not shown for k=2 and k=3 because the vortex is unstable without inflow for these wavenumbers.

a)

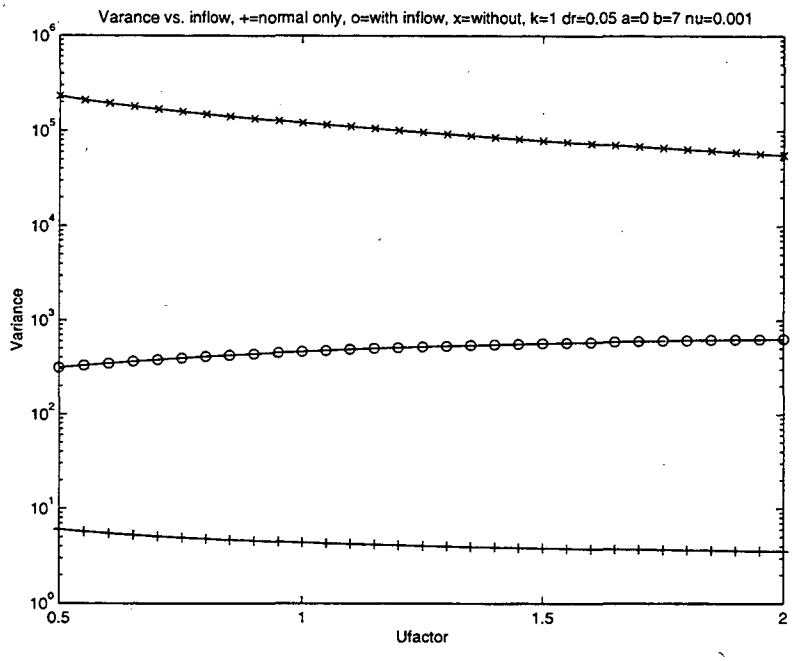

b)

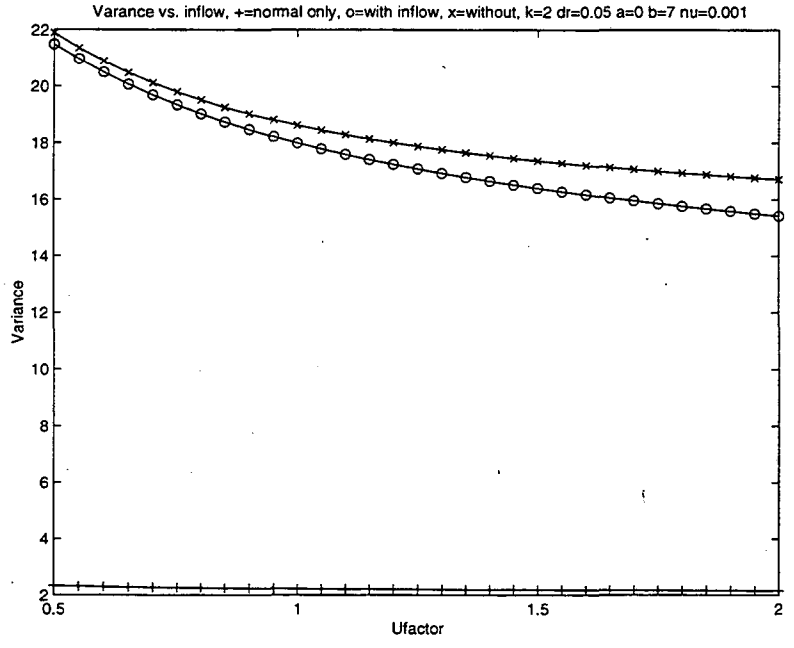

Figure 11 Perturbation variance sustained under unitary stochastic forcing in the one-celled vortex as a function of the strength of the radial inflow, calculated with (o's) and without (x's) the dynamical terms associated with radial inflow, and also for an normal system with the same spectrum (+'s): a) for k=1; b) for k=2.

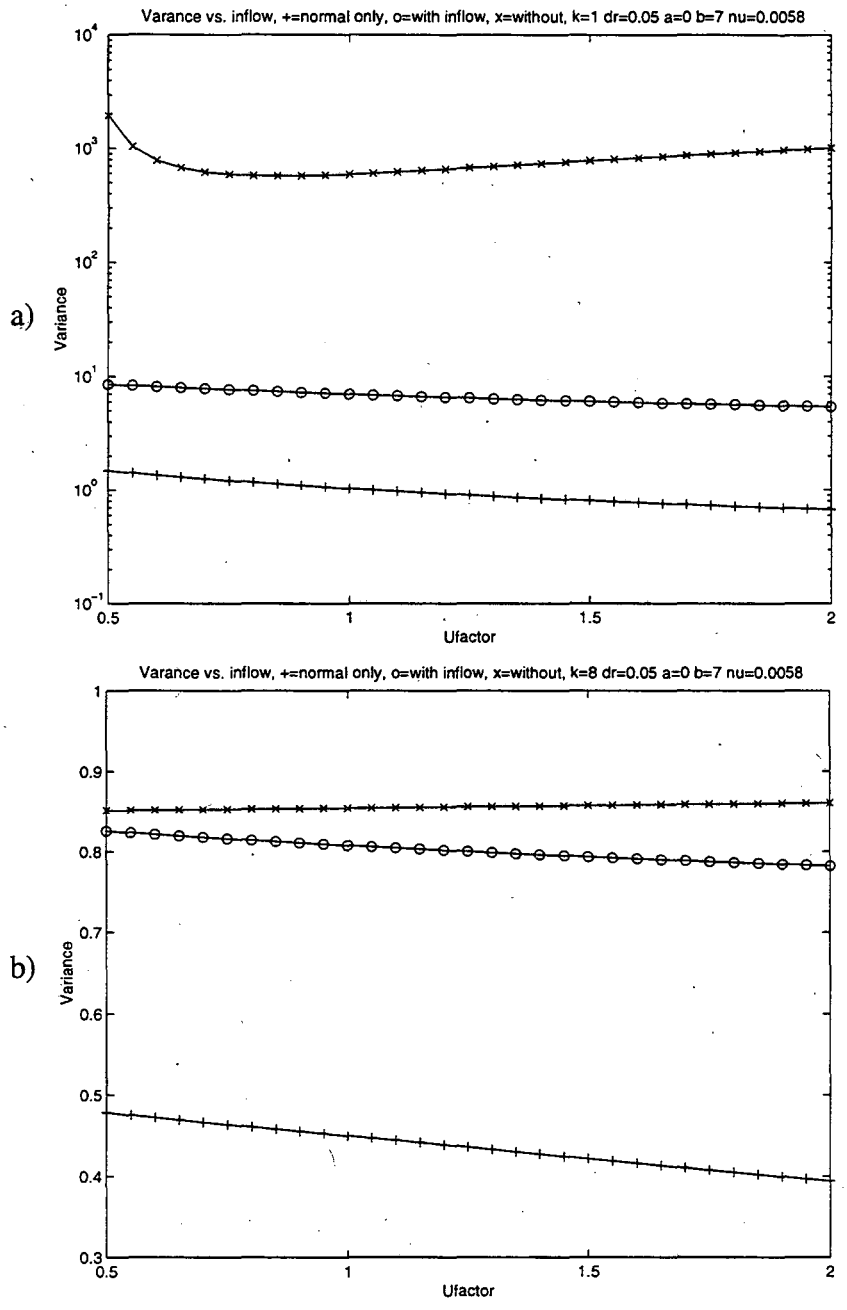

Figure 12 Perturbation variance sustained under unitary stochastic forcing in the two-celled vortex as a function of the strength of the radial inflow, calculated with (o's) and without (x's) the dynamical terms associated with radial inflow, and also for a normal system with the same spectrum (+'s): a) for k=1; b) for k=8.

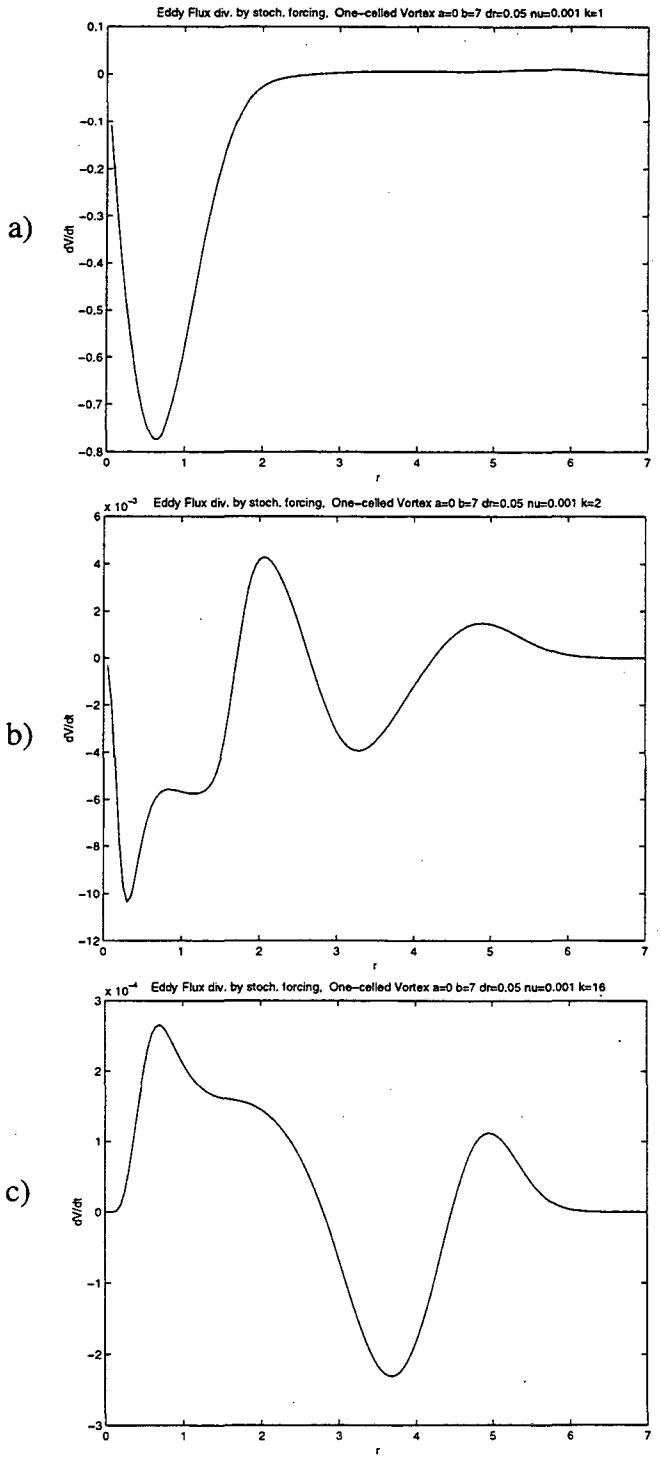

Figure 13 Mean eddy flux divergence caused by perturbations sustained by stochastic forcing in the one-celled vortex: a) for k=1; b) for k=2; c) for k=16.

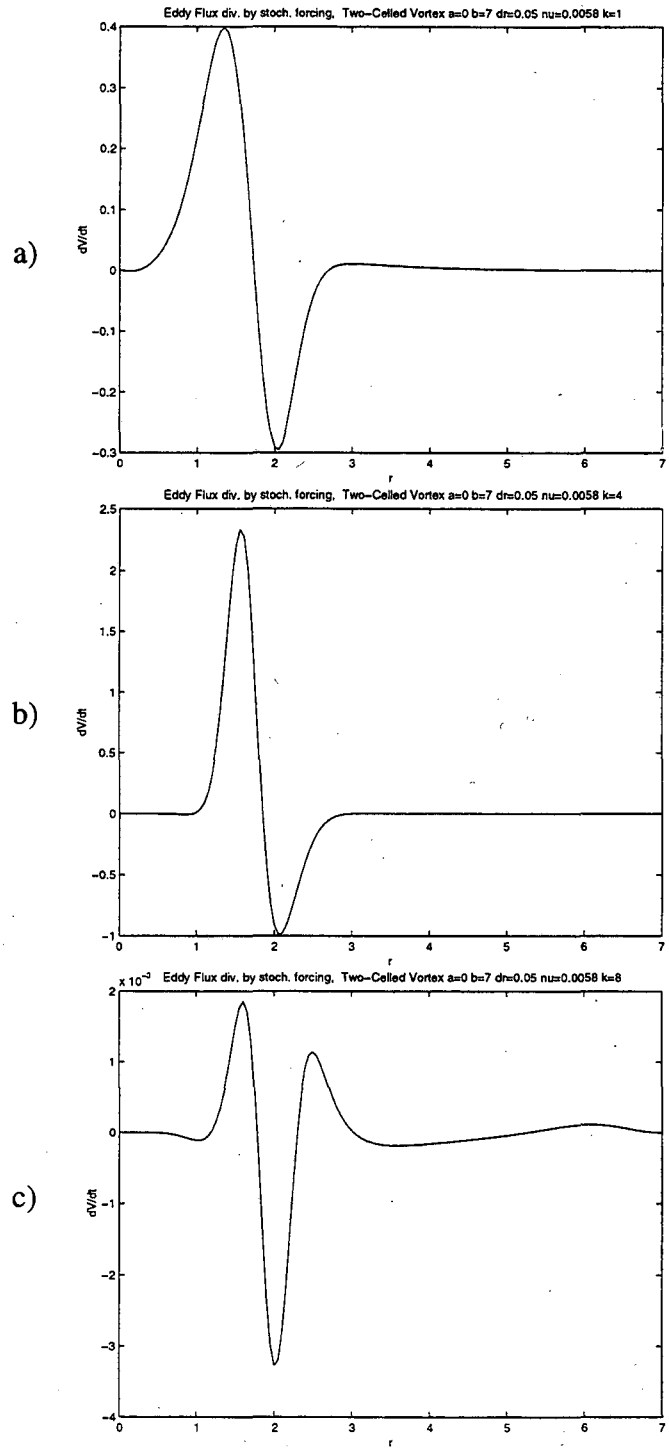

Figure 14 The ensemble-average eddy flux divergences associated with the stochastically maintained perturbations in the two-celled vortex: a) for k=1; b) for k=4; c) for k=8.

a)

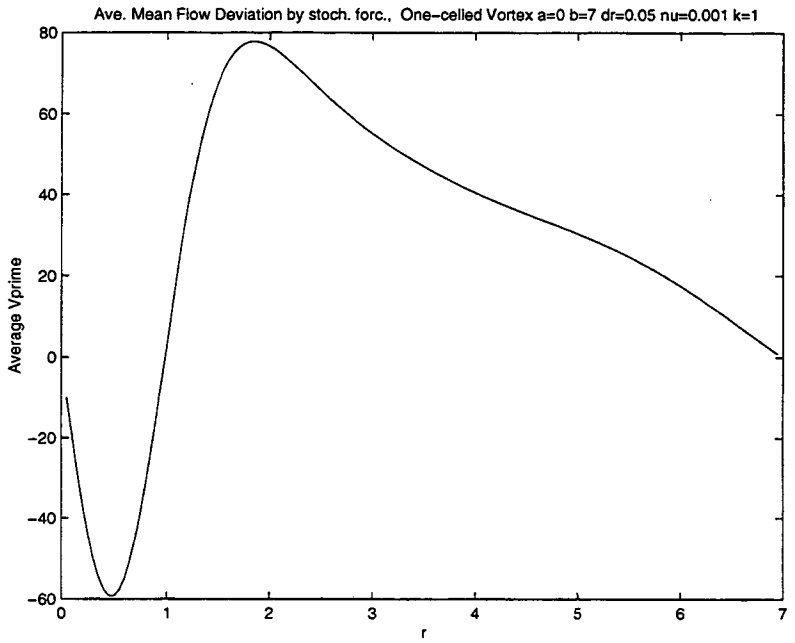

b)

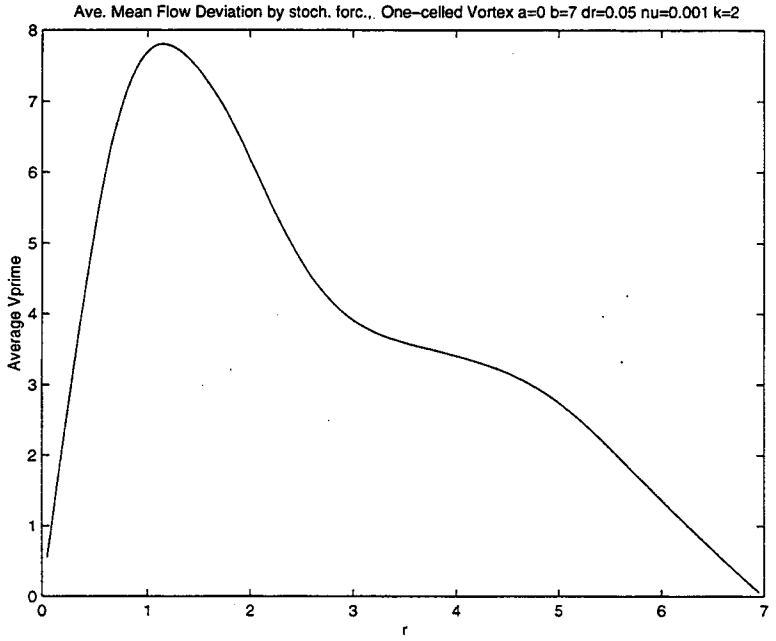

Figure 15 The resulting average mean flow deviations caused by the stochastically maintained eddy flux divergence in the one-celled vortex: a) k=1; b) k=2.

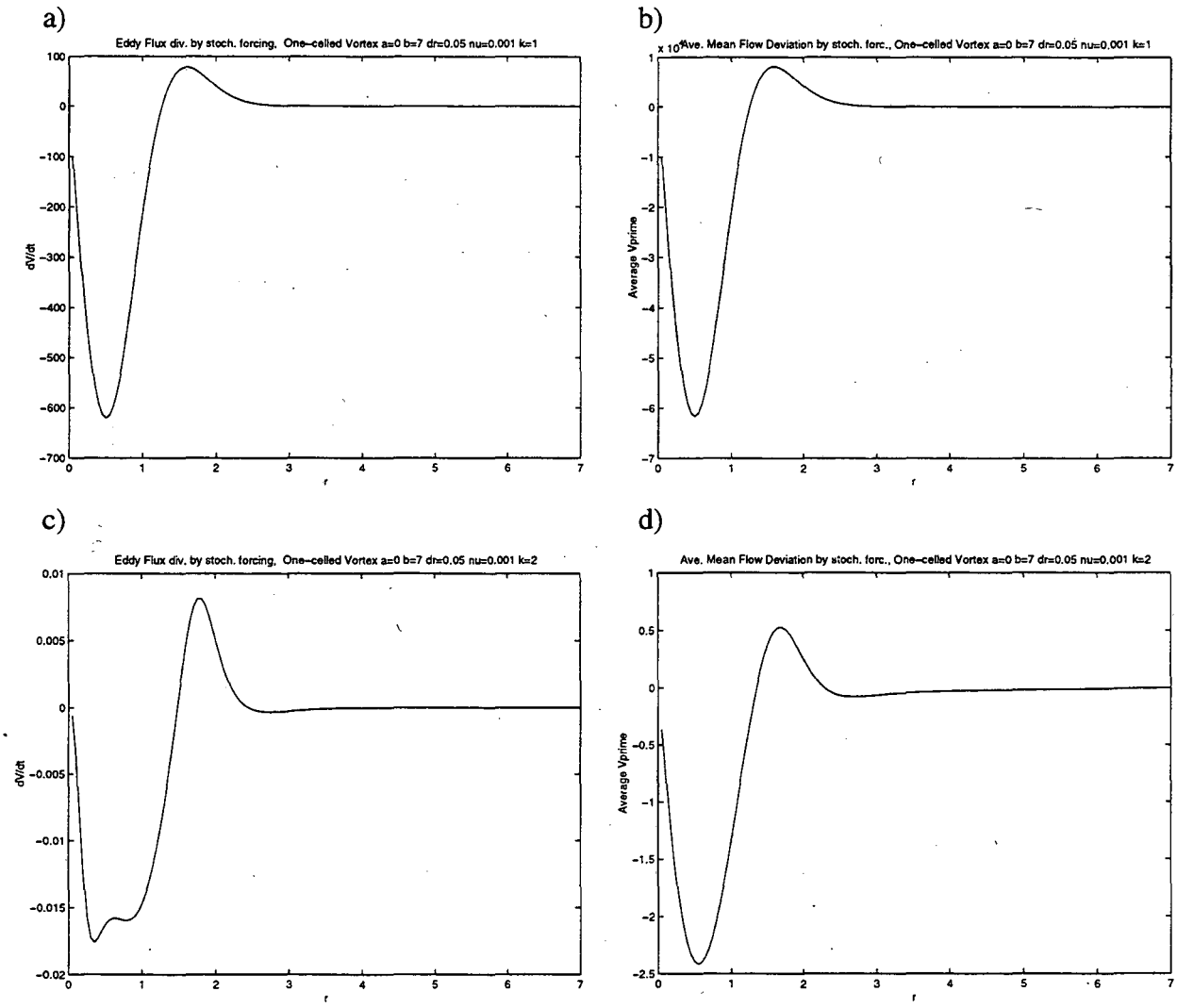

Figure 16 The average eddy flux diverences and resultant mean flow deviations in the one-celled vortex, recomputed with the radial inflow eliminated: a) average eddy flux diveregnce, k=1; b) average mean flow deviation, k=1; c) average eddy flux divergence, k=2; d) average mean flow deviation, k=2.

a)

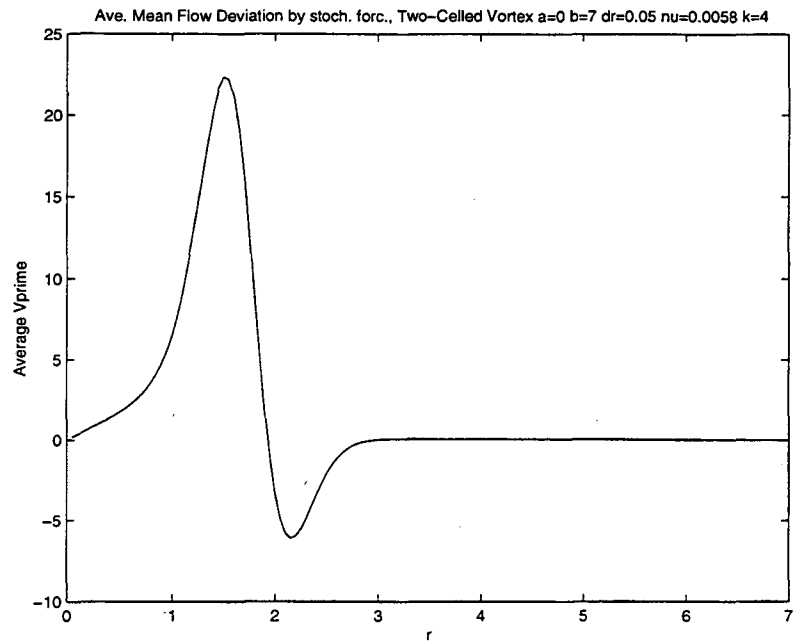

b)

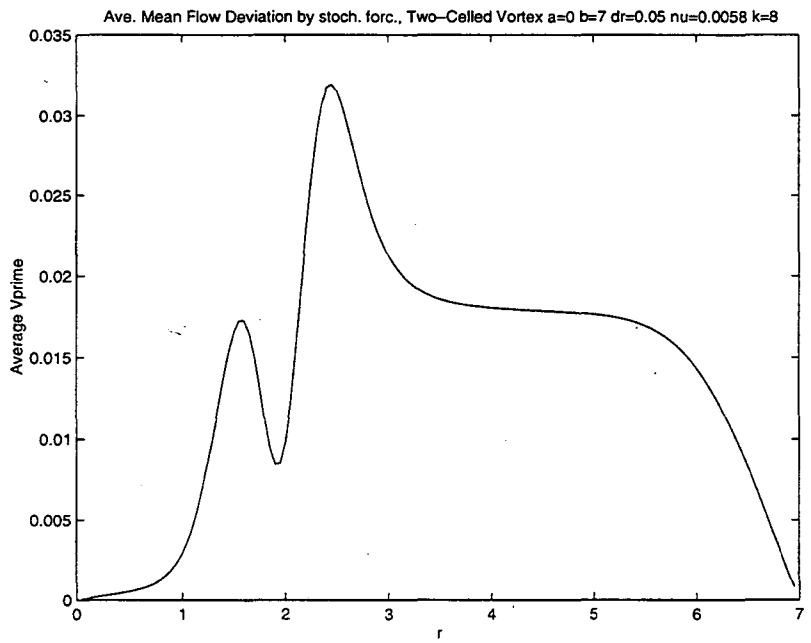

Figure 17 The average mean flow deviations in the two-celled vortex caused by the stochastically maintained perturbations: a) for k=4; b) k=8.

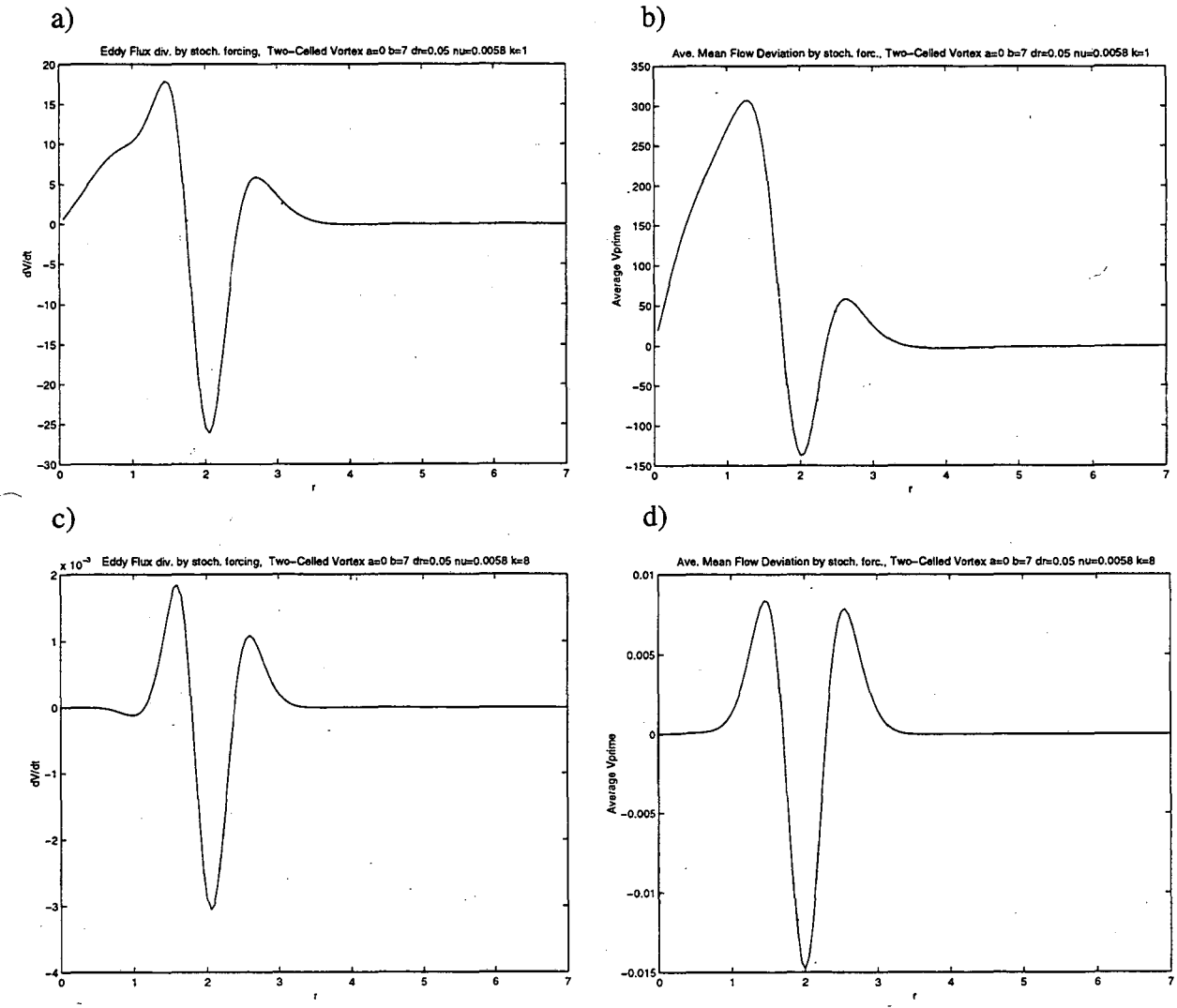

Figure 18 The average eddy flux diverences and resultant mean flow deviations in the two-celled vortex, recomputed with the radial inflow eliminated: a) average eddy flux diveregnce, k=4; b) average mean flow deviation, k=4; c) average eddy flux divergence, k=8; d) average mean flow deviation, k=8.

Ernest Orlando Lawrence Berkeley National Laboratory
One Cyclotron Road | Berkeley, California 94720

Prepared for the U.S. Department of Energy under Contract No. DE-AC03-76SF00098